Physics – Uspekhi **59** (10) 997 – 1020 (2016)

REVIEWS OF TOPICAL PROBLEMS

PACS numbers: **52.35.–g**, 52.35.Hr, 52.35.Qz, 96.60.P–, 96.60.Tf, 97.60.Gb

100th ANNIVERSARY OF THE BIRTH OF V L GINZBURG

Double plasma resonance and its manifestations in radio astronomy

V V Zheleznyakov, E Ya Zlotnik, V V Zaitsev, V E Shaposhnikov

DOI: https://doi.org/10.3367/UFNe.2016.05.037813

Contents

Abstract. **The double plasma resonance (DPR) effect is the phenomenon of a sharply increased instability of plasma waves in a magnetized plasma when the upper hybrid frequency coincides with the cyclotron harmonic frequency. A radiation mechanism associated with this effect provides an explanation for the origin of the 'zebra pattern' in radio spectra of the Sun, Jupiter, and the Crab pulsar. The diversity of these astronomical objects and the successful interpretation of their spectra in terms of the DPR effect point to the universal nature of this phenomenon and suggest that the same radiation mechanism can operate under a variety of astronomical conditions.**

Keywords: solar corona, Jupiter's magnetosphere, Crab pulsar, plasma instability, radio emission

1. Introduction

In plasma physics, the coincidence of the hybrid (upper or lower) resonance frequency with one of the cyclotron harmonic frequencies is referred to as the double plasma resonance (DPR). At the upper and lower hybrid resonance, these frequencies are respectively determined by the plasma electrons and ions (i.e., by the electron or ion plasma frequency and the electron or ion gyrofrequency). The DPR effect consists in the enhanced excitation of plasma waves at the DPR frequencies in nonequilibrium plasma (see paper [1] published in 1966). Conversion of plasma waves into electromagnetic waves leads to intense electromagnetic radiation.

In homogeneous magnetoactive plasmas, the DPR effect clearly arises at one resonance frequency (one harmonic) for a certain relation between the plasma density and the magnetic field strength. But in a regular inhomogeneous plasma, this effect can occur in different plasma layers, i.e., at different harmonics. Ultimately, this gives rise to a system of intermittent stripes in the frequency spectrum of electromagnetic radiation.

Intensive studies of plasma wave instabilities at DPR frequencies started in the mid-1970s [2–5] after the discovery in the dynamic spectra of solar radio emission (the dependence of the emission intensity on time and frequency) of a fine structure in the form of a system of equidistant stripes with enhanced intensity against a broadband background, called the 'zebra pattern' [6, 7]. Observations of the zebra pattern (ZP) in solar radio emission carried out during the last 40 years (see, e.g., [8–34]) and the results of theoretical studies of the DPR effect [10, 22, 23–25, 35–48] favor the association of the ZP with DPR suggested in [2–5].

Later, the ZP was discovered in decameter [49] and kilometer [50] radio emission from Jupiter, in kilometer radio emission from Saturn [51], and in the very low-frequency (VLF) emission from Earth's magnetosphere [52]. These phenomena are also likely to be due to the DPR effect [53, 54]. As regards the ZP in the microwave spectrum of the Crab pulsar, its discovery in 2007 by Hankins and Eilek [55] was quite unexpected and significantly changed our knowledge about the structure of pulsar magnetospheres. Before this finding, theoreticians had believed that the pulsar

V V Zheleznyakov, E Ya Zlotnik, V V Zaitsev, V E Shaposhnikov
Institute of Applied Physics, Russian Academy of Sciences,
ul. Ul'yanova 46, 603950 Nizhny Novgorod, Russian Federation
Tel. +7 (831) 436 35 19
E-mail: zhelez@appl.sci-nnov.ru, zlotnik@inbox.ru,
za130@appl.sci-nnov.ru, sh130@appl.sci-nnov.ru

Received 6 May 2016
Uspekhi Fizicheskikh Nauk **186** (10) 1090 – 1116 (2016)
DOI: 10.3367/UFNr.2016.05.037813
Translated by K A Postnov; edited by A M Semikhatov

magnetosphere formed by a fast-rotating pulsar was fully relativistic. The strong analogy between the ZP seen in the sporadic solar radio emission and the ZP observed in microwave radiation from the Crab pulsar and the successful interpretation of the latter by the DPR effect, which arises only in a nonrelativistic plasma, strongly suggested that the magnetospheric plasma around pulsars also contains local nonrelativistic plasma regions.

Thus, the DPR effect plays a significant role in radio astronomy for the following reasons. First, it has enabled a detailed interpretation of the ZP observed in sporadic solar radio emission. Second, the universal character of this mechanism in diverse astronomical objects has become clear. And finally, in the theory of pulsar radio emission, this mechanism has provided new information on the physical conditions in the magnetospheres of rotating neutron stars.

In this review, we first present the theory of the DPR effect in magnetoactive plasma (Section 2). We then show, using specific examples, how this effect allows explaining different features of the ZP in solar radio emission in different frequency bands (Section 3.1), in kilometer radio emission from Jupiter (Section 3.2), and in the microwave emission from the Crab pulsar (Section 3.3). Section 4 is devoted to modeling the DPR effect in laboratory plasmas.

2. Double plasma resonance effect in magnetoactive plasma

According to [1–5], the instability of plasma waves propagating almost perpendicular to a magnetic field sharply increases at the upper hybrid (plasma) resonance frequency

$$\omega_{\mathrm{UH}} = (\omega_{\mathrm{p}}^2 + \omega_B^2)^{1/2} \tag{1}$$

if this frequency is close to harmonics of the electron gyrofrequency,

$$\omega_{\mathrm{UH}} \approx s\omega_B\,. \tag{2}$$

Here, $\omega_{\mathrm{p}} = (4\pi e^2 N/m)^{1/2}$ is the plasma frequency, $\omega_B = eB/mc$ is the electron gyrofrequency, N is the electron number density, B is the magnetic field, e and m are the charge and mass of the electron, and c is the speed of light. Condition (2) can be realized for many harmonics only in a weak magnetic field where

$$\omega_B \ll \omega_{\mathrm{p}}\,. \tag{3}$$

Then condition (2) reduces to the equality

$$\omega_{\mathrm{p}} \approx s\omega_B\,. \tag{4}$$

If the plasma contains an admixture of electrons with a nonequilibrium velocity distribution, the dispersion properties of the system are mainly determined by the background component, and the instability can be due to the more energetic nonequilibrium electrons. The enhanced plasma wave generation at the DPR levels is due to the electrons that are nonequilibrium in terms of velocities normal to the magnetic field and occurs when these waves propagate almost perpendicular to the magnetic field. This is because at frequencies close to the electron cyclotron harmonics, the waves that propagate at small angles to the magnetic field suffer a strong collisionless decay in the background plasma [57–61]. Therefore, the waves at frequencies close to $s\omega_B$ excited by energetic electrons can exist only in a narrow angle range near $\pi/2$ between the magnetic field and the wave propagation direction.

As is well known [57–61], for a kinetic instability to occur, the plasma wave increment in the background (equilibrium) plasma with an admixture of nonequilibrium particles must have the form

$$\gamma = -\left.\frac{\operatorname{Im}\varepsilon_{\parallel}^{(1)}}{\partial(\operatorname{Re}\varepsilon_{\parallel}^{(0)})/\partial\omega}\right|_{\varepsilon_{\parallel}^{(0)}=0}, \tag{5}$$

where $\varepsilon_{\parallel}^{(0)}$ and $\varepsilon_{\parallel}^{(1)}$ are the respective longitudinal dielectric permeabilities for the background and nonequilibrium components. The DPR effect is caused by an increase in the increment as the frequency ω_{p} approaches $s\omega_B$ due to both nonequilibrium particles [the numerator in (5)] and the dispersion properties of the longitudinal plasma waves in the background plasma [the denominator in (5)].

2.1 Longitudinal cyclotron waves in equilibrium plasma

The dispersion equation for longitudinal waves propagating perpendicular to the magnetic field **B** in equilibrium nonrelativistic plasma with the Maxwellian electron velocity distribution is given by [57–61]

$$\varepsilon_{\parallel}^{(0)} = 0\,, \tag{6}$$

where

$$\varepsilon_{\parallel}^{(0)} = 1 - \omega_{\mathrm{p}}^2 \sum_{l=1}^{\infty} \frac{2l^2 \exp(-\lambda)\, I_l(\lambda)}{(\omega^2 - l^2\omega_B^2)\lambda}\,, \tag{7}$$

$$\lambda = \frac{k_{\perp}^2 v_T^2}{\omega_B^2}\,, \qquad v_T^2 = \frac{\kappa T}{m}\,, \tag{8}$$

$k_{\perp}$ is the component of the wave vector **k** normal to the magnetic field, T is the plasma temperature, $I_l(\lambda)$ is the modified Bessel function of the lth order, and κ is the Boltzmann constant. Equation (6) also approximately holds for the angles α between the magnetic field **B** and the wave vector **k** close to $\pi/2$ in the domain of weak Landau damping:

$$|\omega - l\omega_B| \gg \sqrt{2}\, k_{\parallel} v_T \tag{9}$$

($k_{\parallel}$ is the component of **k** parallel to **B**). The interval of angles α for weakly damped longitudinal waves can be determined by combining inequality (9) with solutions (11) and (12) of the dispersion equation. The result suggests that for any λ, condition (9) is satisfied in a narrow angle interval where $\cos^2\alpha \ll 1$.

If $\lambda = k_{\perp}^2 v_T^2/\omega_B^2 \ll 1$, i.e., the wavelength is much larger than the electron gyroradius, expression (7) reduces to

$$\varepsilon_{\parallel}^{(0)} = 1 - \frac{\omega_{\mathrm{p}}^2}{\omega^2 - \omega_B^2} - \frac{3\omega_{\mathrm{p}}^2\omega_B^2\lambda}{(\omega^2 - 4\omega_B^2)(\omega^2 - \omega_B^2)} - \frac{\omega_{\mathrm{p}}^2}{\omega^2 - s^2\omega_B^2}\,\frac{s}{(s-1)!}\left(\frac{\lambda}{2}\right)^{s-1}. \tag{10}$$

Equation (6) then has solutions at frequencies close to the electron cyclotron harmonics $s\omega_B$ (the so-called Bernstein

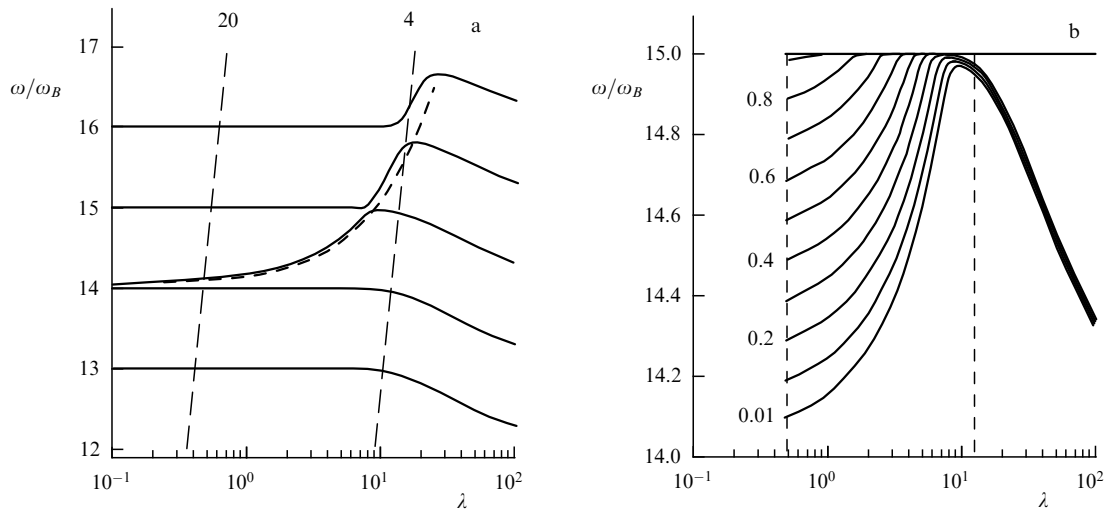

Figure 1. Longitudinal cyclotron waves in equilibrium weakly anisotropic plasma. (a) Dispersion curves in the interval $12 < \omega/\omega_B < 17$ for the detuning $\Delta = \omega_p/\omega_B - 14 = 0.01$; the dashed lines show the instability boundaries for two ratios v_e/v_T of the velocities of nonequilibrium electrons and equilibrium plasma electrons (numbers near the curves); the dashed curve is the approximate dispersion relation. (b) Dispersion curves in the hybrid band $14 < \omega/\omega_B < 15$ for different detunings Δ indicated with numbers; the dashed lines are the same as in Fig. 1a.

modes [57–63]):

$$\omega^2 - s^2\omega_B^2 \approx \frac{\omega_p^2\omega_B^2}{(s^2-1)\omega_B^2 - \omega_p^2}\,\frac{s(s+1)}{(s-2)!}\left(\frac{\lambda}{2}\right)^{s-1}, \qquad (11)$$

and at the frequency near the upper hybrid resonance:

$$\omega^2 \approx \omega_{UH}^2 + 3\lambda\omega_B^2 = \omega_{UH}^2 + 3k_\perp^2 v_T^2. \qquad (12)$$

The closeness of the frequency ω to one of the harmonics or the hybrid frequency allows simplifying Eqn (6) by retaining only the leading terms in the infinite sum ($l = 1, 2$) and the resonance term (with the number $l = s \approx \omega/\omega_B$, $s \geqslant 3$).

The dispersion curves $\omega = \omega(\lambda)$ for longitudinal waves propagating perpendicular to the magnetic field are shown in Fig. 1a for arbitrary λ. The frequency range between the neighbor cyclotron harmonics within which the hybrid frequency $\omega_{UH} \approx \omega_p$ falls is called the hybrid band. The behavior of the function $\omega(\lambda)$ for different ratios $\omega_{UH}/\omega_B \approx \omega_p/\omega_B$ inside the hybrid band is shown in Fig. 1b. Here, the frequency interval $12 < \omega/\omega_B < 17$ and the hybrid band between the harmonics $s = 14$ and $s = 15$ are chosen for illustration because a significant part of ZP events in the solar radio emission are observed at harmonics $s \geqslant 10$.

The DPR effect is present only for waves with normal dispersion at frequencies $\omega > \omega_{UH}$. Clearly, the hybrid band is distinguished among other frequency intervals by the behavior of the dispersion curves for $\lambda < s$: inside the hybrid band, the dependence $\omega(\lambda)$ for $\lambda < 1$ is determined by relation (12), i.e., $\omega \to \omega_{UH}$ as $\lambda \to 0$, while at higher and lower harmonics, with $\omega \to s\omega_B$ as $\lambda \to 0$, it is determined by the last (resonant) term in (10). Thus, dependence (12) holds only inside the hybrid band $s\omega_B < \omega < (s+1)\omega_B$ and cannot be extended to the bands adjacent to the hybrid band from above, although the dashed curve $\omega(\lambda)$ in Fig. 1a, described by approximate formula (12), at first glance is also close to the exact solution for $\lambda > 1$. However, these solutions diverge when approaching the upper boundary of the hybrid band, where the correct function $\omega(\lambda)$ reaches a maximum and decreases as λ increases further.

An analysis (see [2, 42] for more details) shows that the denominator $D = \omega_B\,\partial(\mathrm{Re}\,\varepsilon_\parallel^{(0)})/\partial\omega|_{\varepsilon_\parallel^{(0)}=0}$ in the expression for the increment in the normal dispersion domain (12) is

$$D \approx \frac{2\omega_B}{\omega} \qquad (13)$$

and takes values much smaller than in the adjacent frequency intervals. Moreover, inside the hybrid band itself, D increases in passing from the lower to the upper boundary, which leads to the increment growth [42].

Thus, the role of the equilibrium component in the DPR effect is that inside the hybrid band at frequencies $s\omega_B < \omega_{UH} < \omega < (s+1)\omega_B$ (inside the intervals of the wave vector $k_\perp$ where the normal dispersion occurs), the denominator in (6) for the increment takes values $D \approx 2/s$ that are much smaller than the corresponding values in other frequency intervals between harmonics.

2.2 Instability in electron cyclotron harmonics

When discussing instability, following [2, 3, 37, 59, 60], we consider the velocity distribution of nonequilibrium electrons in the form

$$f(v_\parallel, v_\perp) \propto v_\perp^2 \exp\left(-\frac{v_\parallel^2 + v_\perp^2}{2v_e^2}\right), \qquad (14)$$

where $v_\parallel$ and $v_\perp$ are the longitudinal and transverse components of the electron velocity relative to the magnetic field. Function (14) introduced in [64] describes the characteristic properties of particles trapped by the magnetic field: the deficit of slow velocities and a zero mean velocity along the magnetic field. The distribution over the transverse velocities has its maximum at the velocity v_e with the dispersion $\Delta v_e \sim v_e$. With such a dispersion of velocities of nonequilibrium electrons, the increments attain larger values than for a narrower or wider distribution function [65]. Specific distribution (14) was chosen for explaining the DPR effect because the integrals can be taken explicitly, while for a wider class of distribution functions in the loss-cone form, the result can be obtained only by numerical integration, which often cannot illustrate the essence of the effect.

The numerator of increment (5) is determined by the longitudinal electric permeability due to nonequilibrium electrons [57–61]:

$$\varepsilon_{\parallel}^{(1)} = \frac{2\pi\omega_{\rm pe}^2}{k^2} \sum_{l=-\infty}^{\infty} \int_{-\infty}^{\infty} {\rm d}v_{\parallel} \times \int_0^{\infty} {\rm d}v_{\perp} \, \frac{J_l^2(k_{\perp}v_{\perp}/\omega_B)(k_{\parallel}v_{\perp}\,\partial f/\partial v_{\parallel} + l\omega_B\,\partial f/\partial v_{\perp})}{\omega - l\omega_B - k_{\parallel}v_{\parallel}} \,, \quad (15)$$

where J_l is the lth-order Bessel function and $\omega_{\rm pe}^2 = 4\pi e^2 N_{\rm e}/m$, with $N_{\rm e}$ being the number density of nonequilibrium electrons.

Formula (15) is written in the nonrelativistic approximation, without the relativistic dependence of the electron mass on velocity. The cyclotron resonance, i.e., the pole of the integrand in (15), is then determined by the (longitudinal) electron velocities parallel to the magnetic field, namely, by the term $k_{\parallel}v_{\parallel}$. Hence, in this approximation, the waves must propagate not strictly perpendicular to the magnetic field but at a small angle to the normal. The dispersion properties of plasma waves are described sufficiently well by formula (7) for the strictly normal propagation. The validity of this approximation, its applicability limits, as well as the account for relativistic effects were considered in [2].

For distribution function (14), the imaginary part of $\varepsilon_{\parallel}^{(1)}$ is determined by the pole of the integrand in (15); it is calculated by standard methods and is given by [2, 59, 60]

$$\operatorname{Im}\varepsilon_{\parallel}^{(1)} = \sqrt{\frac{\pi}{2}}\,\frac{\omega_{\rm pe}^2\omega_B}{k_{\parallel}k^2 v_{\rm e}^3} \sum_{l=-\infty}^{\infty} l \exp\left(-z_l^2\right)\left[\delta_l\varphi_l + (\delta_l+1)\zeta\varphi_l'\right] , \quad (16)$$

where

$$z_l = \frac{\omega - l\omega_B}{\sqrt{2}k_{\parallel}v_{\rm e}} \,, \qquad \delta_l = \frac{\omega - l\omega_B}{l\omega_B} \,, \qquad \zeta = \frac{k_{\perp}^2 v_{\rm e}^2}{\omega_B^2} = \lambda\,\frac{v_{\rm e}^2}{v_T^2} \,, \qquad \varphi_l = \exp\left(-\zeta\right) I_l(\zeta) \,, \quad (17)$$

and $I_l(\zeta)$ is the lth-order modified Bessel function.

When the frequency ω is close to one of the harmonics $s\omega_B$, such that $|\delta_s| \ll 1$, $z_{s\pm1}^2 \gg 1$, we can retain only one term with $l = s$ in (17):

$$\operatorname{Im}\varepsilon_{\parallel}^{(1)} \approx \frac{\sqrt{\pi}\,\omega_{\rm pe}^2 s}{\omega_B(\omega - s\omega_B)}\,\varphi_s'(\zeta)\, z_s \exp\left(-z_s^2\right) . \quad (18)$$

Because the denominator in (5) is always positive for equilibrium plasma, the instability (increment $\gamma > 0$) arises if $\operatorname{Im}\varepsilon_{\parallel}^{(1)} < 0$, i.e., if $\varphi_s' < 0$. The function $\varphi_s(\zeta)$ reaches a maximum at $\zeta \approx s^2$. Therefore, the instability condition $\varphi_s' < 0$ reduces to the inequality

$$\zeta \equiv \frac{k_{\perp}^2 v_{\rm e}^2}{\omega_B^2} > \zeta_{\rm cr} \approx s^2 \quad (19)$$

or, in another form,

$$\lambda \equiv \frac{k_{\perp}^2 v_T^2}{\omega_B^2} > \lambda_{\rm cr} \approx \left(s\,\frac{v_T}{v_{\rm e}}\right)^2 . \quad (20)$$

The instability interval is shown on the dispersion curve plots in Fig. 1 for $v_{\rm e}/v_T = 20$ and $v_{\rm e}/v_T = 4$. We note that the instability boundary lies in the normal dispersion domain, where law (12) holds, only if the velocity of nonequilibrium electrons $v_{\rm e}$ sufficiently strongly deviates from the thermal velocity of electrons, for example, for $v_{\rm e}/v_T = 20$. Conversely, for $v_{\rm e}/v_T = 4$, the instability limit lies in the domain where D is quite large, and in this sense the hybrid band is not distinguished among the adjacent Bernstein modes.

The maximum increment at the frequency $s\omega_B$ corresponds to values of $k_{\perp}$ and the parameter λ at which the function φ_s' attains a negative value with the maximum modulus. This is realized for the optimal parameters

$$\zeta^{\rm opt} \approx 2s^2 \quad \text{or} \quad \lambda^{\rm opt} \approx 2s^2\,\frac{v_T^2}{v_{\rm e}^2} \,. \quad (21)$$

Here, the dependence of the increment on $k_{\parallel}$ is described by the function $z_s \exp\left(-z_s^2\right)$. Therefore, for a fixed frequency ω, the increment reaches the maximum at $z_s = 1/\sqrt{2}$, i.e., for the optimal value

$$k_{\parallel}^{\rm opt} = \frac{|\omega - s\omega_B|}{v_{\rm e}} \,, \quad (22)$$

where the frequency $\omega = \omega(k_{\perp})$ can be found from the dispersion law for $k_{\perp} = k_{\perp}^{\rm opt} = (\omega_B/v_{\rm e})\sqrt{\zeta^{\rm opt}} \approx \sqrt{2}(s\omega_B/v_{\rm e})$. The maximum of $\operatorname{Im}\varepsilon_{\parallel}^{(1)}$ over all $k_{\parallel}$ is

$$\operatorname{Im}\varepsilon_{\parallel}^{(1)} \approx \frac{0.4\sqrt{\pi}\,\omega_{\rm pe}^2 s}{\omega_B(\omega - s\omega_B)}\,\varphi_s'(\zeta) \,. \quad (23)$$

This implies that $\operatorname{Im}\varepsilon_{\parallel}^{(1)}$, which is determined by nonequilibrium electrons, also exhibits a resonance as $\omega \to s\omega_B$. We stress that all formulas starting from (18) are valid only under the condition $|\omega - s\omega_B|/\omega_B \ll 1$. They are presented to show the qualitative behavior of the increment and to estimate the instability limits.

Figure 2 shows the dependences of maximal increments [calculated with formulas (21)–(23)] on the frequency ω in the hybrid band $s = 14-15$ for different values of the detuning $\varDelta = \omega_{\rm p}/\omega_B - 14$ and the velocity ratio $v_{\rm e}/v_T = 20$, as well as the dependence of the increment γ on ω for the detuning $\varDelta = 0.01$ in three bands $s = 13, 14, 15$. Here, all significant terms in sum (16) and exact dispersion equation (6) were taken into account to calculate D. It is easy to see that the increment is maximal when $\omega_{\rm p}$ approaches the lower boundary of the hybrid band. Already for $\varDelta = 0.25$, the maximum increment decreases by e times and further decreases with increasing the detuning. We note, however, that the nonrelativistic approximation used above becomes invalid in the frequency range

$$\Delta\omega \sim s\omega_B\,\frac{v_{\rm e}^2}{c^2} \,, \quad (24)$$

adjacent to the harmonics $s\omega_B$ from below. For $s = 14$ and $v_{\rm e}/c = 0.2$, this range occupies almost half the hybrid band: $\Delta\omega \approx 0.5\omega_B$; therefore, the corresponding parts of the curves in Fig. 2a are shown by the dashed line. At the same time, calculations [2, 65] show that the increments calculated in the relativistic approximation do not exceed the values estimated above. In any case, there is a noticeable decrease in the maximal increment when passing from the lower to the upper boundary of the hybrid band: at the lower boundary, the increase in the maximum increment is due to the term $\omega - s\omega_B$ in the denominator of (23), while at the upper

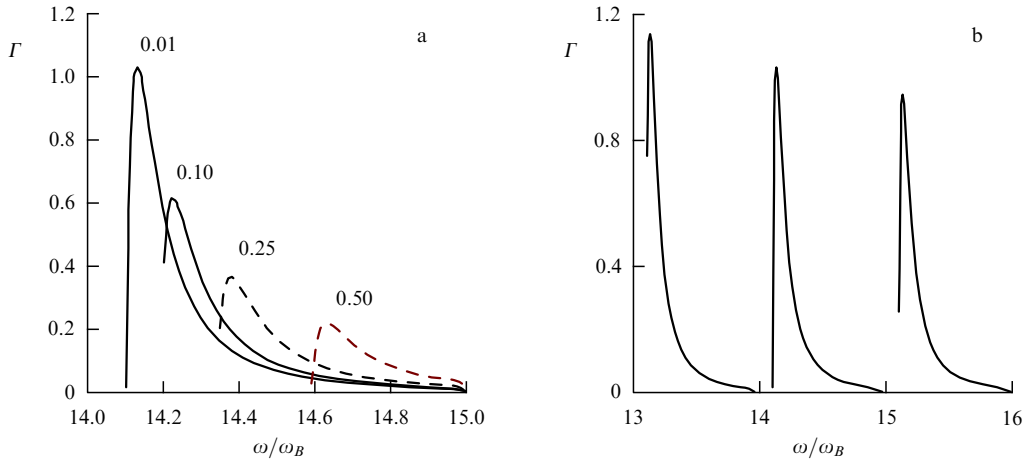

Figure 2. The maximum increment $\Gamma = (\gamma/\omega_B)N/N_e$ as a function of ω: (a) in the hybrid band $14 < \omega/\omega_B < 15$ for different detunings Δ marked with numbers; (b) in three bands $s = 13, 14, 15$ for the detuning $\Delta = \omega_p/\omega_B - 14 = 0.01$; the dashed lines correspond to the parameter region where the nonrelativisitc approximation does not hold.

boundary, this factor is compensated by the increase in the denominator in (7).

That the maximum increment is attained for a small difference between ω_p and $s\omega_B$ enables the resonance effect at $\omega_p \approx s\omega_B$. As seen from Fig. 2, the frequency band with high increments occupies only a small part of the interval ω_B between the harmonics. The maximum increment for optimal angles between the magnetic field and the wave propagation direction, as follows from numerical calculations, is [2, 3, 37, 38, 42]

$$\gamma^{\max} \sim \omega_B \frac{N_e}{N} . \tag{25}$$

As regards the increments in the frequency ranges adjacent to the hybrid band from above, it follows from consistent calculations [42] that they are several orders of magnitude smaller than the corresponding values inside the hybrid band.

Thus, the double resonance effect — a sharp increase in the plasma wave increments when the upper hybrid resonance frequency coincides with a harmonic of the cyclotron frequency — is caused by two main factors. The first is the increment inside the entire hybrid band strongly exceeding those in the neighboring frequency intervals: owing to the dispersion properties of plasma waves, the value of $\partial\varepsilon_{\parallel}^{(0)}/\partial\omega$ at frequencies outside the hybrid band significantly exceeds these values inside it. The decrease in the increment when shifting ω_{UH} from the lower to upper boundary of the hybrid frequency is also due to the increase in $\partial\varepsilon_{\parallel}^{(0)}/\partial\omega$. The second factor is related to the fact that inside the hybrid band, the maximum increment increases at its lower boundary, which is due to the behavior of the function $\varepsilon_{\parallel}^{(1)}$ at the instability values of the wave vector components $k_{\parallel}$ and $k_{\perp}$ that are optimal. It is essential that the DPR effect does not strongly depend on the specific shape of the distribution function of nonequilibrium electrons over velocity components normal to the magnetic field. It is only necessary that this function have a deficit of electrons with low transverse velocities, and the velocity dispersion not significantly exceed the mean velocity. The increment maximum is attained when the mean transverse velocity of nonequilibrium electrons corresponds to the first maximum of the Bessel function in (15), i.e., $k_{\perp}v_{\perp}/\omega_B \sim s$, and the excited waves fall within the normal dispersion domain, where $\lambda = k_{\perp}^2 v_T^2/\omega_B^2 \ll s^2$. These conditions are consistent if $v_e \gg v_T$. Here, both the distribution functions in form (14) and the functions with a loss cone (with the dispersion properties of plasma waves properly taken into account) give rise to enhanced generation of plasma waves in relatively narrow frequency intervals adjacent to the harmonics $s\omega_B$ from above.

2.3 Model of an inhomogeneous radiation source with a quasiharmonic stripe spectrum

We consider the inhomogeneous plasma in which the electron number density and the magnetic field monotonically change along some coordinate x. Then, at each point, the dispersion relations are described by the curves presented in Fig. 1, but when shifting along the x axis (e.g., with changing the electron number density N), the frequency ω_{UH} shifts along the ordinate axis in this figure (for different gradients of the magnetic field and the electron number density). Clearly, the frequency ω_{UH} periodically coincides with cyclotron harmonics, at which the increment sharply increases compared with the frequencies where ω_{UH} is far from $s\omega_B$. It is from these spatially separated parts of the source where $\omega_{UH} = s\omega_B$ that an enhanced emission is expected.

This clearly follows from Fig. 3, which schematically shows how the electron cyclotron frequency harmonics $s\omega_B$ and the upper hybrid frequency $\omega_{UH} \approx \omega_p$ change with the coordinate x in an inhomogeneous source; the regions of the intersection of $\omega_p(x)$ with harmonics $s\omega_B(x)$ (the DPR regions) are marked with circles.

It is easy to see that the emission from such an inhomogeneous system under certain conditions has a frequency spectrum consisting of quasiharmonic stripes with different intensities. If the relation between the magnetic field and the electron number density in the source changes with time, the intersection points in Fig. 3 marking the DPR regions shift along the frequency axis, and the frequencies of the enhanced emission intensity stripes drift.

Figure 3 indicates that the spacing between the stripes

$$\Delta\omega = \frac{s\omega_B L_B}{|sL_B - (s+1)L_N|} \tag{26}$$

is determined by the gyrofrequency and the ratio between the characteristic scales of the plasma number density and

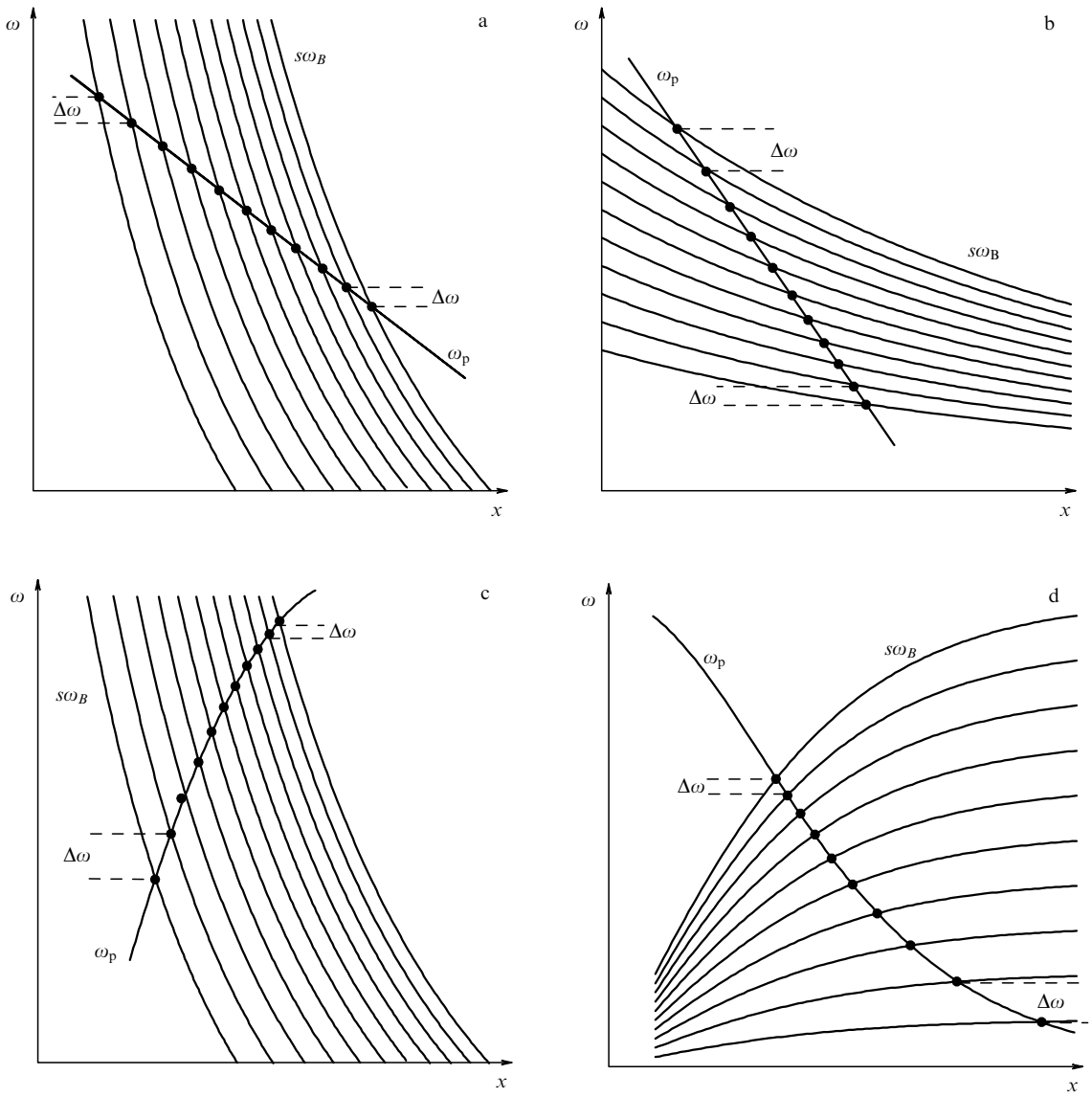

Figure 3. Cyclotron frequency harmonics $s\omega_B$ and the plasma frequency ω_p as functions of the coordinate x along the direction of the change in the layer parameter: (a) for the same signs of L_B and L_N and for $|L_B| < |L_N|$; (b) the same as in panel (a) but for $|L_B| > |L_N|$; (c) for different signs of L_B and L_N and for $L_B < 0$, $L_N > 0$; (d) the same as in panel (c) but for $L_B > 0$, $L_N < 0$.

magnetic field variations [2, 37, 38]:

$$L_B = \omega_B \left(\frac{\mathrm{d}\omega_B}{\mathrm{d}x}\right)^{-1} = B\left(\frac{\mathrm{d}B}{\mathrm{d}x}\right)^{-1}, \tag{27}$$

$$L_N = \omega_p \left(\frac{\mathrm{d}\omega_p}{\mathrm{d}x}\right)^{-1} = 2N\left(\frac{\mathrm{d}N}{\mathrm{d}x}\right)^{-1}. \tag{28}$$

If the magnetic field changes faster than the plasma number density, i.e., $|L_B| \ll |L_N|$ (Fig. 3a), the spacing between the stripes is

$$\Delta\omega \approx \omega_B \frac{L_B}{L_N} \tag{29}$$

and turns out to be smaller than the gyrofrequency. In the opposite case $|L_B| > |L_N|$ (Fig. 3b), the interval between the stripes can be comparable to or higher than the cyclotron frequency. It is very important that, as follows from Figs 3a, b, for the same sign of L_B and L_N, the frequency interval between the neighboring harmonics increases with frequency. By contrast, in the case of opposite signs of these values (Figs 3c, d), the spacing between the bands decreases with frequency.

Thus, a necessary condition for the DPR with multiple enhanced emission stripes to occur is that the plasma is inhomogeneous in the emission generation region and the characteristic scales of the magnetic field and the electron number density are different there. Only in this case can several local regions exist where the relation $\omega_{\mathrm{UH}} \approx s\omega_B$ [Eqn (2)] holds. We also note that in the considered scheme with the same signs of the scales L_B and L_N and $|L_B| < |L_N|$ (Fig. 3a), higher harmonics correspond to lower frequencies of the enhanced emission, and vice versa. In all other cases (Figs 3b–d), the DPR frequencies increase with the harmonic number.

Figure 3 illustrates the location of the DPR regions along some coordinate in an inhomogeneous source. However, in real conditions, the DPR effect occurs on surfaces along which the plasma is inhomogeneous. Clearly, the individual harmonics without overlapping frequencies arise in the emission spectrum only when the DPR surface inhomogene-

ity is sufficiently small (for example, if the part of the surface with nonequilibrium electrons is small).

2.4 Transformation of excited longitudinal waves into electromagnetic waves and polarization of the emission

Plasma waves excited in a source with a sufficiently dense plasma cannot go outside because of strong Landau damping when transiting into rarefied layers on the source boundaries [57–61, 66]. Therefore, the plasma radiation mechanism that is successfully used in interpreting many components of space radio emission necessarily includes a second stage: the transformation (linear or nonlinear) of the longitudinal plasma waves into electromagnetic emission freely escaping from the source.

The transformation mechanisms are described in the literature in detail (see, e.g., [59, 60, 67, 68]). The analysis shows that in astrophysical plasmas, the most effective are the processes of nonlinear convergence of plasma waves, their scattering on plasma particles, or coalescence with low-frequency waves:

$$l + l \to t\,, \qquad \omega_{\rm p} + \omega_{\rm p} \approx 2\omega_{\rm p}; \tag{30}$$

$$l + l_{\rm lf}(i) \to t\,, \qquad \omega_{\rm p} + \omega_{\rm lf} \approx \omega_{\rm p}\,. \tag{31}$$

The last process gives rise to electromagnetic radiation with a frequency slightly different from that of plasma waves, at the so-called fundamental harmonic. The coalescence of two plasma waves generates radiation at the double plasma frequency. This mechanism has been confirmed in the theory of type-II and III solar flares, which explained the observed 1:2 emission frequency ratio [69–72].

Which of the two processes of nonlinear interaction of waves is responsible for the emerging radiation from plasma is difficult to decide from the observed emission intensity. But important information can be obtained if the radiation is polarized. Indeed, in an isotropic plasma, the electromagnetic radiation due to the transformation of longitudinal plasma waves with an isotropic spectrum is unpolarized. In a magnetoactive plasma, the transformation into two normal transversal waves, ordinary and extraordinary, can occur differently depending on the probability of coalescence of the waves (which depends on the magnetic field) and dispersion properties of these modes. Therefore, polarization of the emerging radiation caused by plasma instability (due to the DPR effect in particular) can be determined by different transformation efficiencies of plasma waves as well as by different propagation and escape conditions of ordinary and extraordinary waves from the corona [46].

The spectral intensity of the electromagnetic radiation due to coalescence (3) of two plasma waves with frequencies ω_1 and ω_2, wave vectors k_1 and k_2, and spectral energy densities W_{k_1} and W_{k_2} is given by [67]

$$I_\omega = (4\pi)^4\,\frac{\omega_{\rm p}^3}{c^3}\,\frac{L}{n_{\rm o,e}\left|\partial(\omega^2 n_{\rm o,e}^2)/\partial\omega\right|} \times \int |S|^2 W_{k_1} W_{k_2}\,\delta(\omega-\omega_1-\omega_2)\,\delta(k-k_1-k_2)\,{\rm d}k_1\,{\rm d}k_2 \tag{32}$$

(where L is the source size along the line of sight) and contains coefficients that are different for the ordinary (o) and extraordinary (e) waves. One of them is the quantity $|S|$, a contraction of the nonlinear conductivity tensor that determines the coalescence probability of plasma waves. Another coefficient is the denominator of formula (32), where the refractive indices $n_{\rm o,e}$ are different for normal modes in magnetoactive plasma.

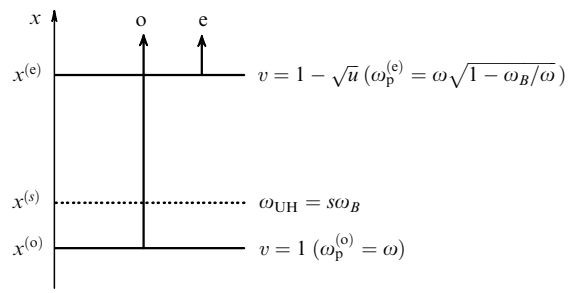

Figure 4. Levels of free escape of the ordinary (o) and extraordinary (e) modes from plasma when propagating along the direction of the plasma number density and magnetic field inhomogeneity; the dashed curve is the DPR level.

Calculations of the probability of the coalescence process under consideration and of the intensity of the emerging electromagnetic radiation for small ratios $\omega_B/\omega_{\rm p}$ are well known in the literature. In particular, it is shown in [73–76] that in a weakly anisotropic plasma with $\omega_B \ll \omega_{\rm p}$, the polarization degree of the electromagnetic radiation at the second plasma frequency harmonic is

$$\rho = A(\alpha, \theta_0)\,\frac{\omega_B}{\omega_{\rm p}}\,, \tag{33}$$

where the coefficient A depends on the angle α between the magnetic field and the wave propagation direction and on the width θ_0 of the angular spectrum of plasma waves. The calculations show that the coalescence of two plasma waves can result in the polarization of the radiation at the double plasma frequency of both normal modes. However, irrespective of the electromagnetic wave polarization sense, the value of A does not greatly exceed unity at any values of α and θ_0. This means that in weakly anisotropic plasma, the degree of polarization cannot be large: $\rho \ll 1$. Thus, if the emerging radiation at the double plasma wave frequency results from the coalescence of two plasma waves, it should not be strongly polarized.

We now consider the possible polarization of electromagnetic radiation at the fundamental frequency resulting from the scattering of plasma waves on plasma ions or from coalescence with low-frequency waves [process (31)]. From general considerations, in the case $\omega_B \ll \omega_{\rm p}$, the difference in the conversion rates into ordinary and extraordinary modes, as well as the dispersion properties of normal modes, lead to a small effect of the order of $\omega_B/\omega_{\rm p}$, i.e., to a low polarization of the emerging radiation. But the difference in the observed emission intensity of normal waves can be due to significantly different escape conditions from the corona of the ordinary and extraordinary waves at frequencies close to the plasma frequency [66, 77, 78]. Indeed, the ordinary and extraordinary waves do not penetrate into the plasma to a depth below which their refractive indices vanish: $n_j^2 = 0$. These regions are located at different levels for the ordinary and extraordinary waves (Fig. 4) and are determined by the following equalities [59, 60, 66]:

$$v = 1\,, \quad \omega_{\rm p}^{(\rm o)} = \omega \quad \text{(ordinary wave)}; \tag{34}$$

$$v = 1 - \sqrt{u}\,, \quad \omega_{\rm p}^{(\rm e)} = \omega\sqrt{1 - \frac{\omega_B}{\omega}} \quad \text{(extraordinary wave)}. \tag{35}$$

The location of these regions is independent of the angle between the magnetic field and the wave propagation direction. In formulas (34) and (35), the standard notation for plasma parameters is used: $v = \omega_{\rm p}^2/\omega^2$ and $u = \omega_B^2/\omega^2$. For simplicity, we consider the waves propagating along the plasma number density inhomogeneity. Then the threshold level $x^{(\rm o)}$ for nondecaying ordinary waves to exist in plasma is always located below the corresponding level $x^{(\rm e)}$ for the extraordinary waves, because $\omega_{\rm p}^{(\rm e)} < \omega_{\rm p}^{(\rm o)}$. This means that if the source of a frequency ω is located above the level $x^{(\rm e)}$, both waves freely propagate in the plasma; the emerging radiation is then nonpolarized. If such a source is located below $x^{(\rm o)}$, both waves decay exponentially in such a dense plasma. If the source is located between these two levels, only the ordinary wave can exit the plasma, and the emerging radiation is then polarized as in the ordinary wave. In a weakly anisotropic plasma, the difference between plasma frequencies at these levels is

$$\omega_{\rm p}^{(\rm o)} - \omega_{\rm p}^{(\rm e)} \approx \frac{\omega_B}{2}\,, \tag{36}$$

which implies that the radiation is polarized as in the ordinary wave if the wave frequency exceeds the local plasma frequency, but by no more than $\omega_B/2$. In a weakly anisotropic plasma, this condition can be satisfied in the DPR regions (see Section 3.1.2 for more details), i.e., in this case the emerging radiation from the source is polarized as in the ordinary wave [46].

Which process, scattering on ions (31) or combinational scattering (30), prevails in the transformation of plasma waves into electromagnetic radiation depends on the energy of plasma waves excited in the DPR regions [59, 60, 79]. The conversion into the fundamental harmonic is effective only for the induced scattering. The character of scattering, spontaneous or induced, depends on the energy density of the excited plasma waves. If the energy density is small, the scattering is spontaneous, and the emission at the second harmonic prevails. This is because plasma waves with oppositely directed wave vectors can participate in the merging process with the emission at the second harmonic. Under the DPR conditions, plasma waves are excited almost normally to the magnetic field, i.e., the wave vectors are located on some disk perpendicular to the magnetic field (more precisely, in a narrow angular interval around this disk). For each wave vector direction, there is always an oppositely directed vector, i.e., the Raman scattering occurs on waves of the subthermal level. The intensity in this case is higher than from the spontaneous scattering of plasma waves on thermal ions into the fundamental harmonic. But if the energy density of plasma waves is sufficiently high, induced scattering occurs, and the fundamental harmonic intensity can be higher than that of the emission at the double plasma frequency.

Thus, studying the polarization of the electromagnetic emission from plasma (and from the DPR regions in particular) can yield important information on the character of the nonlinear transformation of plasma waves into electromagnetic radiation and on the excitation level of plasma waves.

To conclude Sections 2.1–2.4, we note the following necessary conditions for the DPR effect to occur at different cyclotron harmonics in the source of radio emission:

(1) the source must consist of equilibrium nonrelativistic plasma with an admixture of energetic electrons with nonequilibrium velocity components normal to the magnetic field;

(2) the magnetic field must be low enough to ensure that the plasma is weakly anisotropic and the cyclotron frequency harmonics fall within the observed frequency range;

(3) the number density of the equilibrium component must provide the Langmuir frequency in the observed frequency range;

(4) the velocity of nonequilibrium electrons must significantly exceed that of the background plasma electrons but be below the relativistic limit;

(5) the magnetic field and the electron number density in an inhomogeneous source must have different gradients but the same sign.

2.5 Features of the DPR effect on ion cyclotron harmonics

The DPR effect on electron cyclotron harmonics considered above arises when the upper hybrid resonance frequency coincides with electron gyrofrequency harmonics. It can be expected that the same effect arises at low frequency waves when the low hybrid resonance frequency coincides with ion cyclotron harmonics. Such DPR regions can appear in the source only if the lower hybrid resonance frequency is largely determined by the ion number density and the characteristic scales of the magnetic field and ion number density change are different. Below, we show for which parameters the dispersion properties of nonrelativistic equilibrium plasma allow the appearance of the DPR effect with low-frequency waves.

In a homogeneous magnetoactve plasma, ion cyclotron waves are described by the dispersion curves shown in Fig. 1 with the electron cyclotron frequency ω_B replaced by the ion (proton) gyrofrequency $\omega_{B\rm i} = eB/m_{\rm i}c$ ($m_{\rm i} = 1840 m_{\rm e}$ is the mass of a proton, with $m_{\rm e} = m$), and with the upper hybrid resonance frequency $\omega_{\rm UH}$ replaced by the lower hybrid resonance frequency [61, 80]

$$\omega_{\rm LH} = \sqrt{\frac{\omega_{B\rm i}^2 + \omega_{\rm pi}^2}{1 + \omega_{\rm p}^2/\omega_B^2}} = \omega_{B\rm i}\sqrt{\frac{1 + (\omega_{\rm p}^2/\omega_B^2) m_{\rm i}/m_{\rm e}}{1 + \omega_{\rm p}^2/\omega_B^2}}\,. \tag{37}$$

Here, $\omega_{\rm pi} = (4\pi e^2 N/m_{\rm i})^{1/2}$ is the proton plasma frequency and $\omega_{\rm p}$ and ω_B are the respective electron plasma and cyclotron frequencies. For the DPR effect to occur in inhomogeneous plasma, it is necessary that the lower hybrid resonance frequency essentially depend on the plasma number density and, as the magnetic field and the number density change, the hybrid frequency band containing $\omega_{\rm LH}$ shift along the ordinate axis in Fig. 1a from one harmonic to another. We consider under which conditions this is possible.

The second equality in (37) implies that the frequency $\omega_{\rm LH}$ ranges from $\omega_{B_{\rm i}}$ at $\omega_{\rm p}^2/\omega_B^2 \to 0$ to $\omega_{\rm LH} = \sqrt{\omega_{B\rm i}\omega_B} = \omega_{B\rm i}\sqrt{m_{\rm i}/m_{\rm e}}$ at $\omega_{\rm p}^2/\omega_B^2 \gg 1$. This means that the admissible number of harmonics can be sufficiently large:

$$2 < s < \sqrt{\frac{m_{\rm i}}{m_{\rm e}}}\,. \tag{38}$$

It is important that in a plasma that is weakly anisotropic for electrons, with $\omega_{\rm p}^2/\omega_B^2 \gg 1$, the lower hybrid resonance frequency (37), which is equal to $\sqrt{\omega_{B\rm i}\omega_B}$, is independent of the plasma number density, and hence the DPR effect cannot occur at proton cyclotron harmonics. In contrast, in a plasma highly anisotropic for electrons, when the inequalities

$$\frac{m_{\rm e}}{m_{\rm i}} \ll \frac{\omega_{\rm p}^2}{\omega_B^2} \ll 1 \tag{39}$$

hold, where the left-hand side provides the weak ion anisotropy condition $\omega_{\rm pi}^2 \gg \omega_{B{\rm i}}^2$, expression (37) for the lower hybrid resonance frequency reduces to $\omega_{\rm LH} \approx \omega_{\rm pi}$ and, clearly, is determined exactly by the plasma number density variation. Thus, in an inhomogeneous plasma that is strongly anisotropic for electrons ($\omega_{\rm p}^2 \ll \omega_B^2$) and weakly anisotropic for ions ($\omega_{\rm pi}^2 \gg \omega_{B{\rm i}}^2$), the DPR effect can occur if the proton cyclotron harmonics coincide with the lower hybrid resonance frequency:

$$\omega_{\rm pi} = s\omega_{B{\rm i}} \,. \tag{40}$$

Taking this condition into account, it is easy to show that inequality (39) holds for a large number of admissible ion harmonics from interval (38).

Similarly to the case of generation of high-frequency plasma waves excited on the electron DPR in the solar corona, low-frequency longitudinal waves excited on the ion DPR cannot exit the plasma source into the rarefied medium. To overcome the delay zone, these waves must interact with the high-frequency mode. Only in this case is the frequency of the resulting electromagnetic radiation higher than the frequency at which the refractive index of the electromagnetic wave vanishes. Such a high-frequency mode can be a longitudinal plasma wave excited at the upper hybrid frequency $\omega_{\rm UH}$. In the case specified in (39), this frequency is close to the electron gyrofrequency: $\omega_{\rm UH} \approx \omega_B$.

We note that the model of a source based on the DPR effect on ion cyclotron harmonics has one significant difference from the ZP generation source related to the DPR effect on electron cyclotron harmonics. In the latter case, a high-frequency mode instability would be sufficient to produce powerful electromagnetic radiation and the scattering could occur on low-frequency thermal waves or on ions of the equilibrium plasma component. In the case of the DPR effect on ion cyclotron harmonics, both high- and low-frequency modes must be unstable for powerful electromagnetic generation. This is required by the Manley–Rowe relation [68, 81]. For a three-wave interaction process, it implies that the brightness temperature of radiation due to coalescence of high-frequency (hf) and low-frequency (lf) waves is determined by the relation

$$T_{\rm b} \leqslant \frac{(\omega_{\rm lf} + \omega_{\rm hf})T_{\rm lf}T_{\rm hf}}{\omega_{\rm lf}T_{\rm hf} + \omega_{\rm hf}T_{\rm lf}} \,. \tag{41}$$

Therefore, when the low-frequency wave frequency $\omega_{\rm lf}$ is much lower than that of the high-frequency wave $\omega_{\rm hf}$, the radiation temperature is determined by the brightness temperature of the high-frequency mode $T_{\rm hf}$: $T_{\rm b} \leqslant T_{\rm hf}$. This means that if only a low-frequency wave is excited in the source, then, during wave coalescence with the high-frequency thermal mode, thermal electromagnetic radiation is also generated, i.e., no excessive electromagnetic emission or formation of the fine structure of the dynamic spectrum related to the enhanced emission at the ion cyclotron harmonics can be observed. Therefore, the ZP generation scheme with ion cyclotron harmonics must include both the instability at the lower hybrid resonance frequency caused by the presence of an admixture of nonequilibrium ions and the instability at the upper hybrid resonance frequency related to the fraction of nonequilibrium electrons.

We once again stress the astrophysically significant fact that the DPR effect occurs at electron cyclotron harmonics only in a plasma weakly anisotropic for electrons (if $\omega_B^2 \ll \omega_{\rm p}^2$), while the enhanced emission at ion cyclotron harmonics occurs in a plasma strongly anisotropic for electrons ($\omega_B^2 \ll \omega_{\rm p}^2$) and weakly anisotropic for ions ($\omega_{B{\rm i}}^2 \ll \omega_{\rm pi}^2$).

3. DPR effect in the emission from astrophysical objects

In astrophysical plasmas, the necessary conditions for the DPR effect can be satisfied completely. For example, a significant part of the solar corona represents equilibrium weakly anisotropic plasma, and nonequilibrium electrons accelerated during flares and/or trapped by the magnetic field of solar spots can be present in the active regions. In these regions, various plasma instabilities arise, which manifest themselves as bursts of increased (compared to the quiescent background) radio emission from the Sun. In particular, subrelativistic electron beams penetrating the corona give rise to comparatively narrowband and short-lived fast-drifting bursts (so-called type-III bursts) caused by the Cherenkov instability of plasma waves [59, 60, 66, 69–72]. The propagation of the shock in the corona produced by an explosive process gives rise to powerful bursts with a slower drift (type-II bursts) caused by the Buneman instability at the shock front [82, 83]. At the post-flare stage, the increased radio emission is observed as a broadband long-lived continuum (type-IV bursts), which is caused by the instability of electrons with a nonequilibrium distribution of the velocity component normal to the magnetic field [84]. Against this continuum, various kinds of a fine spectral structure are observed as narrowband or short-lived spectral features. One type of such a fine structure, called the 'zebra pattern' by Slottje [7] because of the specific shape of the dynamic spectrum as a set of intermittent bands with increased emission and absorption drifting in time, was successfully explained by the DPR effect. In analogy with the solar ZP, the appearance of similar spectral details in kilometer radio emission from Jupiter and in microwave emission from the Crab pulsar can also be related to the DPR effect.

3.1 Zebra pattern in solar radio emission

3.1.1 Main observational properties of the zebra pattern. The ZP has been recorded for more than 40 years by many solar radio spectrographs in the meter and decimeter radio wave bands [6–13, 22], and in the last decade also in centimeter [14–20, 23–27, 29, 30] and decameter waves [21, 48]. A detailed description of the observational data can be found in reviews [31–34]. Figure 5 shows examples of the dynamic spectra of the ZP in different radio bands. Usually, a ZP emerges at the post-flare stage of solar activity against the type-IV broadband continuum. In dynamic spectra, it appears as equidistant parallel drifting stripes of increased intensity. The typical properties of the ZP in solar radio emission can be summarized as follows:

(1) the lifetime of the ZP in different bursts varies from several seconds to several dozen minutes [7, 8, 13, 22];

(2) the emission brightness temperature $T_{\rm b}$ reaches 10^9 K [22];

(3) the number of stripes varies from a few to several dozen in different bursts [7, 8, 14, 16, 18, 22];

(4) the spacing between the stripes of the pattern is usually less than the radio emission frequency [7, 13, 21–25, 27];

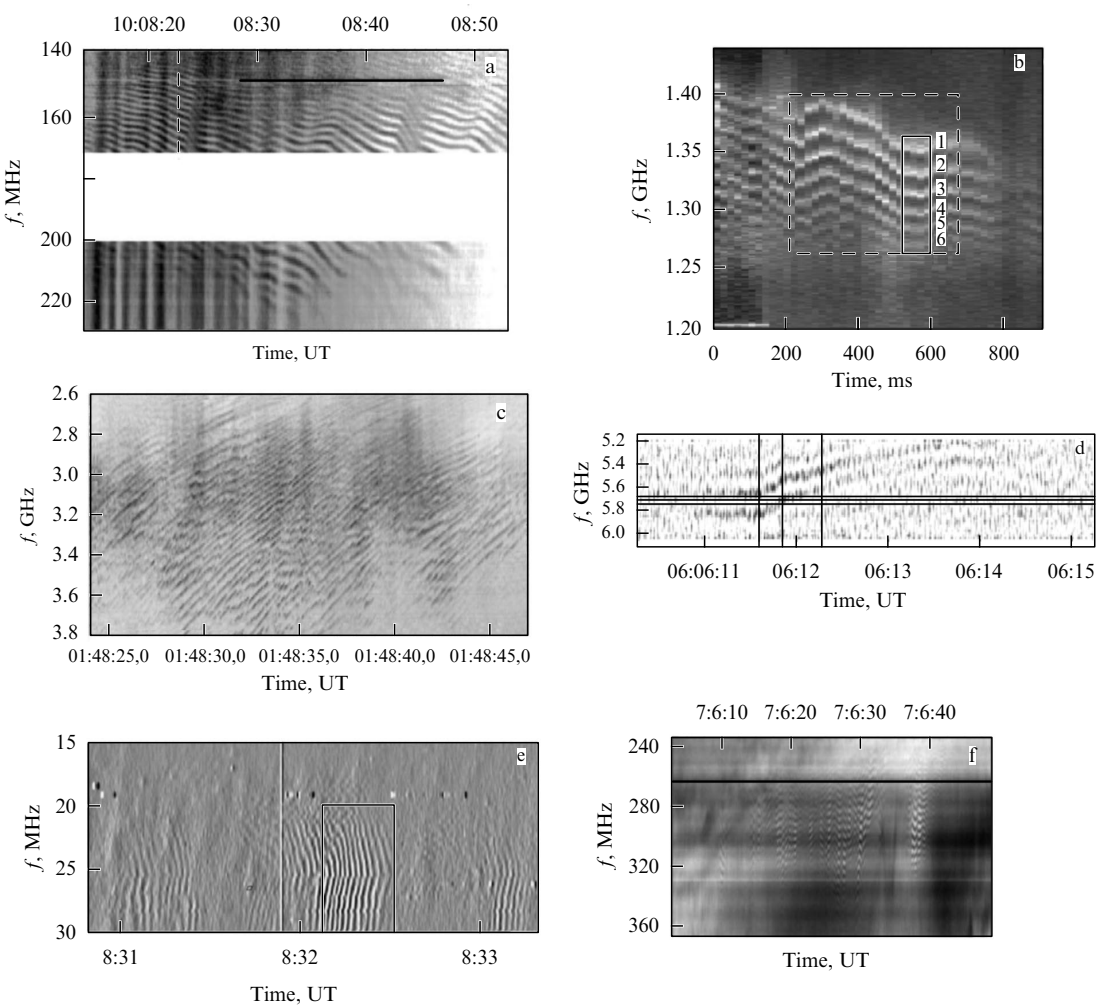

Figure 5. The ZP parameters in the dynamic spectra of solar radio emission detected by radiosphectrographs in different ranges (UT is universal time): (a) 25.10.1994, meter wave range [13]; the dashed curve marks the time for which the ZP source model shown in Fig. 7 is constructed; (b) 14.12.2006, decimeter wave range [22]; (c) 21.04.2002, microwave range [14]; (d) 22.07.2004, decameter wave range [21, 48]; the rectangle shows the part of the spectrum for which the ZP source model in Fig. 8 is constructed; 17.08.1998, meter–decimeter wave range [92].

(5) the stripe spacing in most cases increases with frequency [7, 12, 13, 22]; in the microwave range, the ZP stripes are sometimes equidistant [15];

(6) the emission is strongly polarized, with the sense of polarization corresponding to the ordinary wave, with rare exceptions [9, 11, 31];

(7) the frequency drift sometimes has a wavy character [13, 22];

(8) a superfine structure is sometimes observed against the ZP in the form of quasi-periodic brightness variations [7, 18, 20, 28, 34].

Among ZP observations, observations by Chen et al. [22] in a broad frequency range with high frequency and spatial resolution are of special importance (see the spectrum in Fig. 5b). In that paper, direct evidence is obtained that different ZP stripes are generated in a magnetic flux tube in spatially separated sources. As is shown below, that paper provides the decisive observational argument favoring the ZP origin due to the DPR effect in the solar corona.

3.1.2 Spectral features of the zebra pattern due to the DPR effect. The fine structure of the frequency spectrum and the observed high brightness temperature of emission suggest a coherent radiation mechanism related to the excitation of electromagnetic waves in a nonequilibrium plasma system. Moreover, a relatively long duration of bursts with a ZP implies that increased radiation is produced by electrons localized in the sources (with ring-type or loss-cone transverse velocity distributions) and not by flying electrons, which relatively rapidly escape from the source. This distinguishes type-IV emission with a ZP from short-lived type III bursts and other fast-drifting bursts related to electron beams propagating along magnetic field lines in the corona.

The theory of the ZP origin based on the DPR effect was proposed and developed in a series of papers [2–5] and later developed in [10, 13, 18, 22, 36–48]. As stated in Section 2, a ZP is generated in a distributed source — a magnetic tube or trap with captured electrons whose energy exceeds that of electrons in the equilibrium plasma (Fig. 6). The multi-stripe dynamic spectrum in this model is due to the enhanced emission generation in spatially separated regions where DPR condition (4) holds.

The generation of enhanced ZP radiation in solar radio emission caused by the DPR effect is possible only under special conditions. In addition to the requirements listed in Section 2 [weak anisotropy of equilibrium plasma ($\omega_{\rm p} \gg \omega_B$), different values L_B and L_N of the same sign [see (27) and (28), where the coordinate x plays the role of the height in the

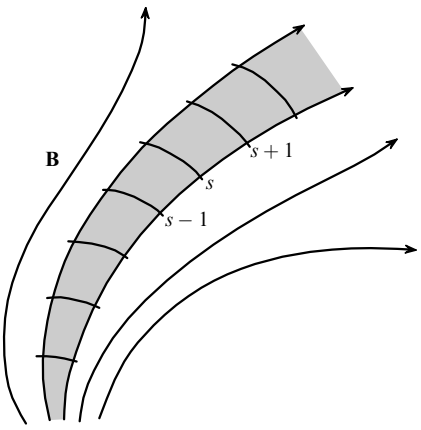

Figure 6. Possible configuration of the ZP source in an active region of the solar corona; the plasma region with the admixture of nonequilibrium electrons is shown in gray [4].

corona], and a significant excess of the mean velocity of nonequilibrium electrons over the mean thermal velocity of electrons in the background plasma ($v_e \gg v_T$)], it is also necessary that increment (25) for kinetic instability at the DPR be higher than the plasma wave decrement due to electron–proton collisions in the coronal plasma $|\gamma_{\rm coll}|$:

$$|\gamma| = \omega_B \frac{N_e}{N} > |\gamma_{\rm coll}| = \frac{\nu_{\rm ei}}{2} \,. \tag{42}$$

Here, the effective number of electron–proton collisions is described (at a temperature $T > 4\times10^5$ K) by the formula [66]

$$\nu_{\rm ei} = \pi \frac{e^4}{(\kappa T)^2} v_T N \ln\left(10^4 \frac{T^{2/3}}{N^{1/3}}\right) \approx \frac{5.5N}{T^{3/2}} \ln\left(10^4 \frac{T^{2/3}}{N^{1/3}}\right) \tag{43}$$

(in the last term, the temperature T is expressed in Kelvin and the number density N in cm^{-3}). This implies that the threshold number density of nonequilibrium electrons that is necessary for the DPR instability to appear is

$$N_e^{\min} \approx \frac{3sN^2}{\omega_p T^{3/2}} \ln\left(10^4 \frac{T^{2/3}}{N^{1/3}}\right) . \tag{44}$$

In the coronal conditions, this value is not high: for example, for the ZP shown in Fig. 5a for the coronal plasma number density $N = 2\times10^8$ cm^{-3} ($\omega_p = 2\pi\,130$ MHz) and the corona temperature $T = 2\times10^6$ K, the threshold number density for harmonics $s = 10-20$ is $N_e^{\min} \approx (0.5-1)\times10^{-6}N$, i.e., only $(1-2)\times10^2$ cm^{-3}. These values are about two orders of magnitude lower than the corresponding values for the kinetic instability in the Bernstein modes [2, 3] and one order of magnitude smaller than required for the loss-cone instability [84].

It is worth mentioning that, originally, two types of DPR instability were proposed to interpret the ZP: kinetic [2, 4] and hydrodynamic [5] instabilities. However, the latter is possible only for a sufficiently narrow velocity distribution of nonequilibrium electrons, which highly constrains the number density of nonequilibrium electrons. Estimates show that even in the most favorable conditions, this number density should be unrealistically high [4, 10]: $N_e^{\rm hd} \gg (\pi/2)s(v_e/c)^4 N \sim 10^{-2}N = 2\times10^6$ cm^{-3} (for $N = 2\times10^8$ cm^{-3}, the optimal velocity of nonequilibrium electrons $v_e/c \approx 0.3$, and harmonic numbers $s = 10-20$ adopted in [2, 4, 37, 38] for the ZP). Thus, the threshold number density of nonequilibrium electrons required for the kinetic instability, $N_e^{\min} \approx (1-2)\times10^2$ cm^{-3}, is four orders of magnitude lower than for the hydrodynamic instability.

Calculations of increments shown in Fig. 2 confirm the enhanced plasma wave generation in narrow frequency intervals in the DPR regions. These calculations were done for distributions of electron velocities normal to the magnetic field in form (14), where the velocity dispersion is close to the velocity itself, $\Delta v_\perp \sim v_\perp$. For a more narrow distribution function, intervals of λ and ω with high increments are smaller than in the case considered [65]. The resonance effect also holds for the so-called loss-cone velocity distribution, although the authors of numerical calculations [37, 38, 47] came to the opposite conclusion. Their statement about the overlapping of neighboring harmonics (and hence about the absence of resolved enhanced-emission bands in that case) is based on an incorrect use of the dispersion properties of the background plasma (when calculating the denominator D in increment (5); see [42] for more details). For loss-cone distributions, enhanced increments are also found in a narrow frequency interval adjacent to the lower boundary of the hybrid band. This means that the ZP in solar sources can be generated by a wide class of nonequilibrium electron distributions.

According to Section 3.3, the frequency spacing between the ZP stripes depends on the gyrofrequency and the degree of inhomogeneity of the coronal plasma and the magnetic field in the DPR source. It is defined by relation (26) or, taking into account that the magnetic field changes in the corona faster than the electron number density ($|L_B| \ll |L_N|$), by formula (29). In this case, the stripe spacing can be significantly smaller than the gyrofrequency ω_B, which is indeed observed in most events with the ZP. Moreover, the diagram shown in Fig. 3a, which is realized in the coronal trap, suggests that this model naturally explains the nonequidistant zebra stripes, i.e., the increase in spacing between the bands with increasing frequency. Such a growth is possible if the values L_N and L_B have the same sign, for example, B and N decrease with increasing height, as usually occurs in the solar atmosphere (see the diagrams in Fig. 3a, b). In the opposite case, i.e., when the signs of L_N and L_B are different, the frequency spacing between stripes decreases as the frequency increases (Fig. 3c, d). It is important to note that if $|L_N| \ll |L_B|$ (Fig. 3b), a situation is possible where the distance between harmonics remains almost unchanged with changing the frequency, which means that the equidistance of a given ZP is not an argument against the DPR-based model.

We next consider the possibility of explaining the large number of stripes observed in some events with the ZP. As already noted, the number of stripes changes from a few to several dozen. The above considerations imply that the number of DPR surfaces in the source is determined, first, by the interval of heights inside which the trapped electrons are localized and, second, by the distance between stripes, i.e., by the value of the magnetic field and characteristic scales of the field and electron number density changes with height. In real conditions of coronal magnetic tubes, the diversity of the number of observed ZP stripes is quite explicable. The almost identical brightness of a large number of bands is questionable, although the maximal increment determined by the function $s\varphi_s'(\zeta)$ in (23) varies with the harmonic number. However, the maximum absolute value of the negative

function $s\varphi_s'(\zeta)$, which determines the increment maximum, decreases with the harmonic number very slowly. This is illustrated by Fig. 3c, which shows the frequency dependence of the increment when the upper hybrid resonance frequency is close to harmonics with $s = 14, 15, 16$. In sources showing a large number of bands, the condition that the increment exceeds the decrement due to collisions is well satisfied for high harmonics. The instability arising at gyrofrequency harmonics is accompanied by the effects of quasilinear relaxation of the fast electron distribution function. The quasilinear relaxation decreases the fast electron velocity component normal to the magnetic field (the normal Doppler effect) and thus tends to suppress the instability due to the filling of the loss cone of the magnetic trap by fast particles. On the other hand, electrons in the loss cone escape from the magnetic trap. The loss cone is partially cleared, and this process sustains the instability. Because the duration of the ZP usually significantly exceeds the characteristic time of the quasilinear relaxation and the lifetime of fast particles in the trap, there should be a source of fast particles in the corona that would compensate the loss of fast particles from the trap. As a result, a balance among the quasilinear relaxation, the resumption of the instability due to loss of particles, and the particle refilling from the source is established. In this quasistationary regime, the efficiency of excitation of plasma waves is no longer determined by linear increments, and plasma waves for different harmonics are excited up to saturation. This fact apparently explains the weak dependence of the ZP stripe intensity on the harmonic number, although this issue requires more detailed studies.

The frequency drift of the ZP on the dynamic spectrum in the model shown in Fig. 3 is due to a change in the magnetic field relative to the electron number density or vice versa. Here, all DPR points shift; therefore, the stripe frequencies vary in the same way, and enhanced emission stripes appear on the dynamic frequency spectrum that undergo a parallel drift as time progresses. We imagine that the electron number density in Fig. 3a remains constant in time and the magnetic field decreases. Then the system of curves $s\omega_B(h)$ shifts down along the frequency axis, and the intersection points with the curve $\omega_{\rm p}(h)$, i.e., the DPR points, move towards higher frequencies. This means that the magnetic field decrease in time leads to a frequency drift, which is indeed observed in most ZP events at the post-flare stage of solar activity. This stage is apparently accompanied by the destruction of magnetic structures and a magnetic field decrease. Of course, the DPR model also allows a negative frequency drift caused by the magnetic field increase or the electron number density decrease with time.

Dynamic spectra of the ZP frequently demonstrate a wave-like behavior of frequency stripes. As shown in [39, 43–45], such a behavior can be related to fast magnetosonic oscillations of coronal magnetic loops in which ZP sources are located. We note that the geometry of ZP levels is determined by the coronal plasma and not by the admixture of fast particles, and can therefore be preserved for a long time. This explains the preservation of quasiharmonic stripes in the dynamic spectral structure for minutes or hours in some observed events.

The observed high degree of polarization of the ZP is also naturally explained by the DPR model [46]. As shown in Section 2.5, high polarization (with the ordinary wave sense) of electromagnetic radiation is due to induced scattering of plasma waves excited at the DPR frequencies on coronal plasma protons or due to coalescence of the excited plasma waves with low-frequency waves. Here, the generation of emission at the frequency $\omega_{\rm pl}$ should occur between the levels where the refractive indices of ordinary and extraordinary waves vanish: $n_{\rm o,e} = 0$ (see Fig. 4, where the x coordinate plays the role of the height h in the solar magnetic tube). The frequency $\omega_{\rm pl}$ of plasma waves excited at the DPR level h_s,

$$\omega = \omega_{\rm pl}(h_s) \approx \omega_{\rm p}(h_s) + \frac{\omega_B^2(h_s)}{2\omega_{\rm p}(h_s)} + \frac{3}{2}\,\frac{k_\perp^2 v_T^2}{\omega_{\rm p}(h_s)}\,, \tag{45}$$

exceeds the local plasma frequency $\omega_{\rm p}(h_s)$. Therefore, the level $h_{\rm o}$ (where $n_{\rm o} = 0$) determined from the condition

$$\omega = \omega_{\rm p}(h_{\rm o}) \tag{46}$$

is located more deeply in the corona than the level h_s. Estimates in [46] show that under the typical ZP generation conditions, the difference between frequencies $\omega_{\rm p}(h_{\rm o})$ and $\omega_{\rm pl}(h_s)$ in (45) is smaller than $\omega_B/2$, and hence, according to Section 2.4, the DPR level is located between the levels $h_{\rm o}$ $(v = 1)$ and $h_{\rm e}$ $(v = 1 - \sqrt{u}\,)$ (see Fig. 4). If the finite width of the frequency interval in which plasma waves are excited and the frequency decrease during plasma wave scattering on ions and their transformation into electromagnetic radiation are taken into account, the generation level of waves with the frequency ω remains within the interval of heights between $h_{\rm o}$ and $h_{\rm e}$ [46].

Thus, the emission produced by scattering on ions of plasma waves excited at the DPR levels turns out to be polarized with the sense of an ordinary wave, which fully corresponds to observations of the ZP in solar flares.

3.1.3 Specific examples of the use of DPR for the diagnostics of physical conditions in the coronal plasma. We consider the dynamic spectrum of 25.10.1994 shown in Fig. 5a and show, following [39], that its characteristics agree with the ZP generation by the DPR effect. The active region NOAA 7792 that is related to this event has been studied in many papers [13, 39–45, 85–88]. Simultaneously with the dynamic spectrum registration by the radiospectrograph in Potsdam, the event was observed by the radioheliograph in Nançay, which allowed localizing the meter-wave radio source in one of the branches of a coronal loop. The radio measurements were supplemented with the optical data on magnetic fields at the photosphere level, the H_α-image of the active region, and soft X-ray observations. These data enabled extrapolation of the photosphere magnetic field to coronal heights. The force-free magnetic field model turned out to provide the best fit to the active region configuration. Knowledge of the coronal magnetic field along a chosen field line allowed the authors of [39] to construct the dependence of the cyclotron harmonic frequencies sf_B [1] on height. According to the layout presented in Fig. 3a, the minimal magnetic field (at the loop top) corresponds to the maximum harmonic number. The extrapolated minimal field is $B_{\rm min} = 1.76$ G at the height $h = 66{,}750$ km. On the dynamic spectrum of the event at 10:08:23 UT, which is chosen in [39] for a ZP analysis and marked with the dashed line in Fig. 5a, the minimal frequency of the zebra stripe is 136.9 MHz. Hence, it is easy to find the

[1] Hereinafter, when comparing the theory with observational data, we use the frequency $f = \omega/2\pi$ instead of the angular frequency ω.

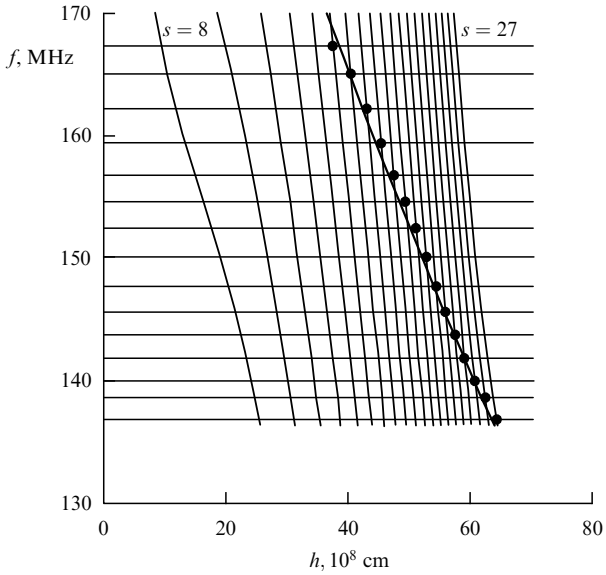

Figure 7. Model of the ZP source based on the DPR theory for the dynamic spectrum in Fig. 5a [39]. The horizontal lines correspond to the ZP stripe frequencies at the time 10:08:23 UT (the dashed line in Fig. 5a); the grid of gyroresonance harmonics $s = 11-27$ is constructed from the results of optical measurements of the photosphere magnetic fields extrapolated to the ZP source location; the intersection points mark the DPR regions; the line connecting these points is the plasma frequency $f_{\rm p}$ distribution with the height corresponding to the barometric coronal plasma number density with the temperature $T \approx 1.2 \times 10^6$ K.

highest harmonic in the ZP at this time, $s = 27$, and to conclude that 15 stripes seen in the instant ZP spectrum correspond to harmonic numbers $s = 13-27$. Figure 7 presents the plot of frequencies of these harmonics versus height along the chosen magnetic field line and shows the zebra-stripe frequencies observed at 10:08:23 UT with horizontal lines. The crossing points of the horizontal lines with the system of harmonics determine the DPR levels, and the line connecting these points represents the electron number density distribution along the height in the magnetic trap. This distribution closely follows the barometric law $N \propto \exp(-2h/10^4 T)$ with the temperature $T = 1.2 \times 10^6$ K. We stress that the height distribution of the electron number density was obtained using two independent data sets: the measured ZP emission frequencies and the magnetic field distribution over height extrapolated from the optical data. This example shows that the ZP was produced in this case exactly by the instability at the DPR levels in the magnetic trap.

The oscillating character of zebra stripes in the dynamic spectrum in Fig. 5a is also explained by the DPR mechanism: according to the generation scheme in use, the drift points to a periodic change in the frequency $f_{\rm p}$ relative to the cyclotron harmonics sf_B or vice versa (see Fig. 3). As shown in [43, 44], this effect is due to fast magnetosonic oscillations of the flux tube in which the ZP source is located. Here, the observed oscillation period is $T \approx 5$ s and its dependence on the harmonic number is in good agreement with the DPR model of the source elaborated in [39].

A similar quantitative model with the reconstructed electron number density along height was developed in [22] for the dynamic spectrum of 14.12.2006 shown in Fig. 5b. Along with the results of positional measurements [22], which showed that different ZP stripes are generated in spatially separated sources, the proposed models of the sources undoubtedly confirm the DPR effect in the coronal conditions.

The next example of a complicated ZP in solar radio emission, which we discuss as a manifestation of the DPR effect in the solar corona, was recorded by the UTR-2 spectrograph in Kharkov (Ukraine) in the frequency range 14–30 MHz (Fig. 5e) [21, 48]. The observed structure is reminiscent of a fingerprint and differs from the ordinary ZP at meter and decimeter wavelengths by exhibiting a frequency drift of different signs within one frequency band at a fixed time instant. At first glance, the dynamic spectrum shown here can hardly be related to a ZP. Here, not enhanced emission stripes with equidistant frequencies but quasiperiodic bursts of enhanced emission are observed, i.e., a fine temporal structure, but not a frequency structure, and it is difficult to interpret it as a typical ZP in terms of the DPR effect.

A characteristic feature of the fingerprint dynamic spectrum is the fast drift of zebra stripes, with the drift direction changing to the opposite inside one harmonic. This means, first, that the changes in the characteristic scales of the magnetic field and electron number density should be close (to provide a small number of the observed zebra stripes at a fixed time) and, second, the relation between these two scales in the upper and lower parts of the source should be opposite. The model of the source proposed in [48] is presented in Fig. 8a: the electron number density distribution in the source is described by a small deviation from the commonly accepted Newkirk model of a coronal ray [89], and the magnetic field varies along the height at a rate similar to the electron number density change rate. The frequency drift of zebra stripes is caused by the magnetic field decrease in time and motion along the curves corresponding to the values of sf_B in Fig. 8a. The infinite drift velocity is attained at times when one of the harmonics $sf_B(h)$ touches the curve $f_{\rm p}(h)$. Figure 8b, which shows a comparison of the calculated and observed frequencies of zebra stripes for the detail marked with the rectangle on the dynamic spectrum in Fig. 5e, suggests that the proposed model well explains the fingerprint spectral features of the burst.

In the microwave range, many events with the ZP are also due to the DPR effect. The dynamic spectrum shown in Fig. 5c provides an example. It exhibits a large number of zebra stripes and a variation of the interstripe distance with frequency, which is typical for the DPR mechanism. As regards the superfine structure of the ZP, which represents quasiperiodic brightening and dimming of emission inside one stripe [7, 18, 20, 28, 32, 34], it can be caused by peculiarities of the periodic nonlinear regime of excitation and transformation of plasma waves generated at DPR levels [90, 91].

The DPR can explain even more complicated behaviors of zebra stripes found in some spectra. For example, papers [90, 92] report on events in which a ZP appears only in fast-drifting shells similar in form to type-III solar radio bursts (Fig. 5f). As shown in [92], such a structure can be explained by the DPR effect by assuming that the plasma contains an admixture of nonequilibrium electrons with a specific distribution over the longitudinal and transverse velocity components with respect to the magnetic field.

Thus, a detailed examination of specific ZP events allows us to show how the DPR effect can be used to explain features of the ZP under the realistic solar corona conditions and how

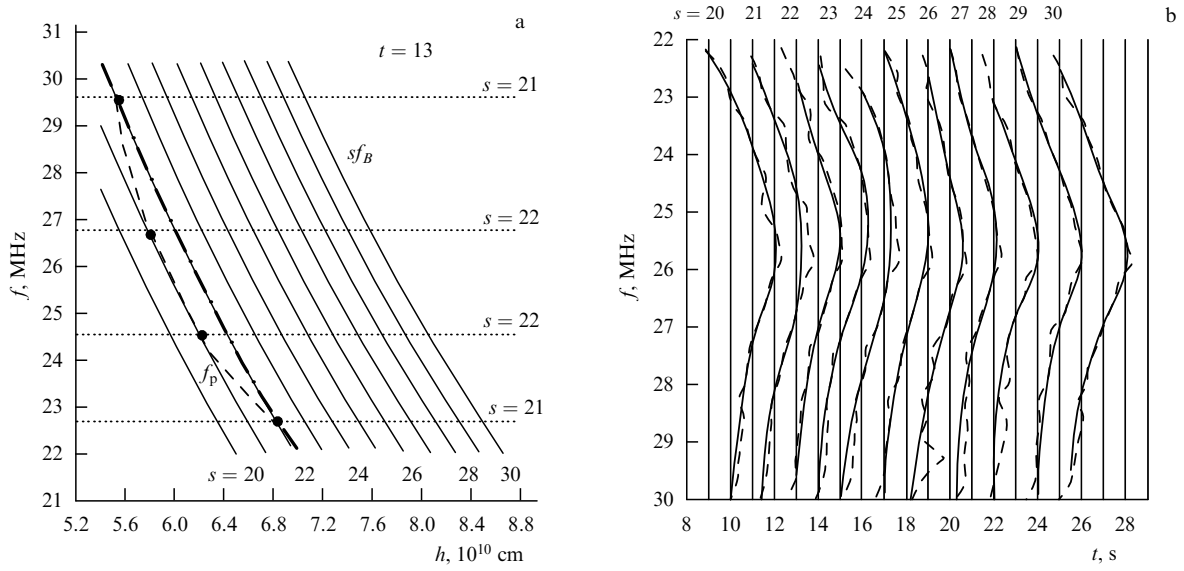

Figure 8. Model of the source of a fingerprint burst [21, 48] for the dynamic spectrum in Fig. 5e. (a) The height distribution of the plasma frequency f_p (dashed-dotted curve: the Newkirk model [89]; dashed line: deviation from the Newkirk model proposed for the fingerprint burst source) and the height distribution of cyclotron harmonics sf_B (solid lines) at $t = 10{:}32{:}13$ UT; horizontal lines are the observed zebra stripe frequencies at that time instant. (b) Digital form of the dynamic spectrum fragment selected with a rectangle in Fig. 5e: the observed (dashed lines) and calculated (solid lines) frequencies f of the ZP stripes in the fingerprint burst model [48]; the figures on the top mark the gyrofrequency harmonic number corresponding to the ZP stripes.

the proposed theory can be used to probe physical conditions in the emission sources.

The above considerations suggest that DPR effectively operates in the solar corona and gives rise to the ZP in dynamic spectra of solar radio emission. However, it is not possible to state that absolutely all ZP events are due to the DPR effect. In particular, the origin of the burst shown in Fig. 5d [14], which demonstrated a few stripes with a relatively large stripe spacing and synchronous frequency change, is incompatible with the model of a distributed DPR source. The authors of [14] interpret the observed features by the generation of longitudinal cyclotron modes (Bernstein modes) in a homogeneous magnetic field.

The idea that the ZP represents emission produced by the coalescence of plasma waves at the frequency f_p and Bernstein modes at the gyrofrequency harmonics sf_B was suggested in [93, 94]. Later, mechanisms of the Bernstein mode instability in nonequilibrium plasma and of their nonlinear coalescence with plasma waves were elaborated in [2, 3, 14, 15, 20, 29, 35, 95]. Clearly, this scheme can explain only dynamic spectra with strictly equidistant bands and cannot explain the usually observed change in the frequency spacing between stripes as the frequency changes. In addition, for most of the meter and decimeter ZP events, the magnetic field determined by the interstripe spacing equal to f_B turns out to be unrealistically low for coronal sources.

3.1.4 Analysis of alternative mechanisms of the origin of zebra patterns in solar radio emission. Different theories proposed in the literature to explain ZPs without invoking the DPR effect can be subdivided into three main groups [41, 96].

(1) The mechanism proposed in [97] uses the effect of capture of plasma waves by local plasma density enhancements. The authors assume that plasma waves excited in a local source at a frequency close to $2f_B$ or $3f_B$ have anomalous dispersion (the wave frequency decreases with the wave number). Here, the limited volume of the source provides a discrete frequency spectrum of standing plasma waves. However, this mechanism cannot explain the observed feature of ZP spectra, in particular, the broad frequency range within which ZPs are observed (see [17, 41, 96] for more details). In addition, the requirements that the emission source be compatible with the observed ZP properties (the size of the plasma wave trap of about a few meters, the relative change in the number density $\Delta N/N \approx 20\%$, and the number of such traps at about 10^8 with fully identical parameters of the magnetoactive plasma in these traps) look unrealistic for the solar corona conditions [41, 96].

(2) The next large group of papers suggesting a ZP interpretation is related to the excitation of low-frequency electromagnetic waves — so-called whistlers — in the solar corona (see reviews [31–34] and the references therein). Whistler (w) and longitudinal (l) plasma waves at the plasma frequency are assumed to be excited by a system of nonequilibrium electrons with a loss-cone-like velocity distribution, and the observed radio emission arises during nonlinear coalescence of these waves: $l + w \to t$, $\omega = \omega_p + \omega_w$.

Whistlers seem to be appealing in interpreting ZPs because their frequency $\omega \ll \omega_B$ can be adjusted to the interstripe distance in the observed ZP. But if we assume that there is a high-frequency continuum and the interaction of an excited whistler with a plasma wave gives rise to an enhanced emission and absorption band, this can explain the emergence of only one filament but not the harmonic structure of the spectrum. To obtain a quasiharmonic system of ZP stripes, it is necessary to assume that in the system with a high-frequency continuum, whistlers are excited in some regions spatially separated by height intervals providing approximately equidistant bands on the dynamic spectrum. Unlike the scheme involving the presence of DPR levels in the source, which are due to the geometry of the trap and always exist for different variability scales of the magnetic field and the electron number density with height, the existence of the

enhanced whistler level at special heights looks difficult to realize.

The above papers assume that the quasilinear and nonlinear (periodic in time) regimes of excitation of whistlers in a trap and features of their propagation along ducts lead to the splitting of the trap into an enhanced whistler energy zone and their absorption zone. But the stratification of the trap by passing waves requires solving a complicated nonlinear problem of excitation and propagation of whistlers in an inhomogeneous source and fitting many parameters (see [41] for more details). This problem has not been posed or solved.

Thus, the theory based on the role of whistlers in the ZP origin meets with serious objections. At the same time, whistlers, along with other low-frequency waves, can well be significant in the interaction with Langmuir waves in models involving the plasma mechanism of the ZP origin. But in this case, the harmonic structure of the spectrum is determined by the features of generation of high-frequency waves and not whistlers: in the interaction of two waves, the brightness temperature of the resulting emission is determined by Manley–Rowe relation (41), and for $\omega_{\rm w} \ll \omega_{\rm p}$, the value of $T_{\rm b}$ depends weakly on the brightness temperature of the low-frequency component $T_{\rm w}$ and almost coincides with that of the high-frequency plasma wave, $T_{\rm b} \approx T_{\rm p}$.

(3) Yet another group of papers explains the ZP origin not by the features of the emission generation in the source itself but by the effects of propagation of electromagnetic waves through the corona. The reason for the appearance of the spectrum with alternating bands of enhanced and low intensity is assumed to be the effects of interference or diffraction of electromagnetic waves that arise for a specific configuration of sources in the corona [98, 99], or wave propagation through a spatially periodic medium, which may filter incident radiation by forming frequency transparency and opacity windows [100–103].

A common shortcoming of all these models is that they do not pose the question of the origin of the initial monochromatic electromagnetic emission that should be produced in a point-like source. Next, the interference or diffraction pattern can arise only from the interaction of coherent waves, whereas waves with random phases propagate in the coronal plasma. Moreover, to provide the observed ZP intensity, the number of such identical sources located at one height in the corona and acting coherently should be unrealistically high (for example, 10^6 according to [98]). Nor does the solution of the problem of wave propagation through periodic structures resolve the situation: first, the existence of a periodic structure of unclear origin with a period of about 3–30 m (which is required to reproduce the observed characteristics) during a long time interval is hardly possible in the solar corona, and second, the frequency transparency and opacity windows have different sizes for ordinary and extraordinary waves [103], which means that the ZP stripes must be smeared out in nonpolarized emission measurements, contradicting observations. We note in conclusion that the problem setting itself in [100–103] is ill-defined: the authors substitute the solution of the problem of the origin of periodic structures in the radio emission spectrum by hypothetical assumptions on the existence of periodic inhomogeneities in the corona.

3.2 Zebra pattern in kilometer wave emission from Jupiter

Kilometer radio emission from Jupiter was first observed during the flights of the Voyager 1 and 2 spacecraft in 1979. A large amount of information on this emission was obtained by the Cassini mission in 2000. A structure similar to the ZP in solar radio emission was discovered in the 25–75 kHz frequency range [50]. The dynamic spectrum shown in Fig. 9 represents a set of equidistant bands of enhanced intensity drifting parallel in time. The figure suggests that the frequency interval between the stripes is much smaller than the frequencies themselves and increases as the frequency increases.

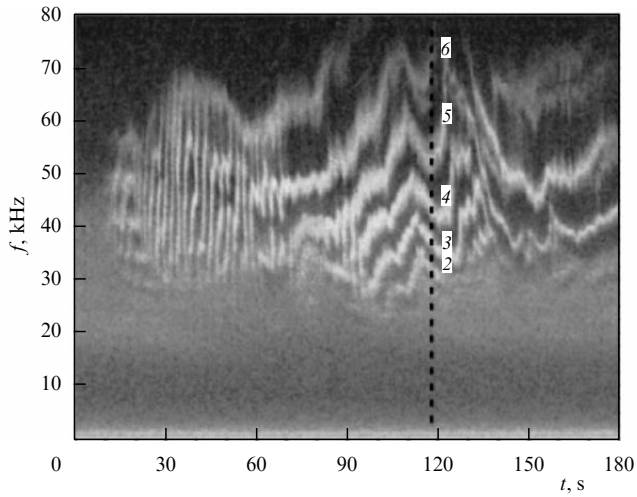

Figure 9. Dynamic spectrum with a ZP in the kilometer radio emission from Jupiter [50]; the dashed line marks the time at which the ZP shown in Fig. 10 is constructed.

The analogy between ZPs in radio emission spectra of the Sun and Jupiter suggests that the mechanisms responsible for the origin of equidistant stripes in the spectra can be the same in both cases, i.e., the observed spectrum can be the manifestation of DPR in Jupiter's atmosphere. To interpret the ZP in the kilometer radio emission of Jupiter, the idea of the total similarity between this structure and the solar ZP was proposed in [53], where the enhanced emission was assumed to arise in regions where the upper hybrid resonance frequency coincides with the electron cyclotron harmonics. As pointed out above, the DPR effect in this case can occur only in weakly anisotropic plasma. Therefore, a model of the source was suggested in [53] such that the DPR region and emission sources with the ZP are located in the equatorial current sheet layer (with an increased plasma number density) along magnetic field lines belonging to the L-shells from the interval $10 \leqslant L \leqslant 10.5$ (where $L = R_L/R_{\rm J}$, $R_{\rm J}$ is Jupiter's radius and R_L is the distance from the center of the planet to the crossing of a magnetic field line with the equator). This interval of the L-shells is found by fitting the calculated spectrum (in the VIP4 magnetic field model [104]) to the observed one, i.e., by comparing the model cyclotron harmonic frequencies with the observed zebra-stripe frequencies. To be compatible with observations, the plasma number density in the ZP sources should be two times as high as that in the known model [105].

In the model in [53], the electron number density increases and the magnetic field decreases when moving towards the equator along an inhomogeneous source elongated along the magnetic field line, i.e., the quantities L_B and L_N have different signs. In the proposed model, the calculated interstripe spacing should decrease with frequency, which contradicts observations. According to Figs 4c, d, when the

signs of L_B and L_N are opposite, the distance between bands should decrease with frequency. For this distance to increase with frequency, as in the spectrum shown in Fig. 9, the quantities L_B and L_N should have the same signs (Fig. 3a, b). In addition, according to measurements [106], in most of Jupiter's magnetosphere, the plasma is strongly anisotropic ($\omega_B \gg \omega_p$). Therefore, another interpretation of the ZP in the kilometer radio emission of Jupiter was proposed in [54] based on the DPR effect on ion cyclotron harmonics.

As shown in Section 2.5, this effect is possible only in a strongly anisotropic plasma ($\omega_p \ll \omega_B$) under the condition that $\omega_{pi} \gg \omega_{Bi}$ for ions. Here, the lower hybrid resonance frequency coincides with the ion plasma frequency, $\omega_{LH} \approx \omega_{pi}$, and the dispersion properties of ion cyclotron waves are described by the curves shown in Fig. 1 with the substitution of ω_B by ω_{Bi} and ω_{UH} by ω_{LH}, and the enhanced generation of ion cyclotron waves occurs at ion DPR levels: $\omega_{pi} = s\omega_{Bi}$. This implies that the source must be located outside the equatorial current sheet, where the plasma is weakly anisotropic ($\omega_p \gg \omega_B$). According to [54], the source is located in Jupiter's atmosphere on the shell $L = 15$ at latitudes of 40–50 degrees. It consists of an equilibrium electron–proton plasma with an admixture of energetic electrons and protons trapped by the magnetic field with nonequilibrium transverse velocity components relative to the magnetic field. The source is elongated along the magnetic field line. In such a source, an instability of plasma waves arises at upper and lower hybrid resonance frequencies with a continuous spectrum. In addition, under these conditions, the DPR effect on ion cyclotron harmonics is possible.

In [54], the model of the source is constructed as follows (Fig. 10). The magnetic field is assumed to correspond to the VIP4 model [104]. In this magnetic field, the dependences of the electron gyrofrequency f_B (the upper part of the figure) and the ion cyclotron harmonics sf_{Bi} (the lower part of the figure) for $s = 2-6$ are calculated as a function of the relative distance $r = R/R_J$ to the center of Jupiter (the choice of harmonics $s = 2-6$, the shell $L = 15$, and the latitude interval of the source are justified in [54]). The horizontal lines mark the observed frequencies of zebra stripes at a given time shown by the dashed line in Fig. 9. Because the expected zebra-stripe frequencies $f = sf_{Bi}(r) + f_B(r)$ are close to $f_B(r)$, the crossing points of the horizontal lines with the curve $f_B(r)$ determine the location of the ZP sources on the r axis; the corresponding distances $r = R/R_J$ are marked with stars on the abscissa axis. Clearly, the intersection of the vertical lines with harmonics $sf_{Bi}(r)$ determine the ion cyclotron harmonic frequencies at the DPR points; they are marked with filled circles on the $sf_{Bi}(r)$ curves. The solid line connecting these crossing points determines the required behavior of the ion plasma frequency.

The instability at the upper hybrid resonance frequency $f_{UH}(r) \approx f_B(r)$ in an inhomogeneous source gives rise to enhanced emission with a continuous spectrum. Superimposed on this continuum, at frequencies $f(r) = sf_{Bi}(r) + f_B(r)$, are bands with enhanced brightness due to nonlinear coalescence of low-frequency waves at the DPR frequencies $sf_{Bi}(r)$ and high-frequency waves at frequencies $f_B(r)$. The required intervals of the plasma number density in the sources obtained from the function $f_{pi}(r)$ in Fig. 10 are $N_e = N_i \approx (0.03-1.3)$ cm^{-3}. The magnetic field for the observed frequency range 25–75 kHz and harmonics $s = 2-6$ must range within $B \approx (1-2) \times 10^{-2}$ G.

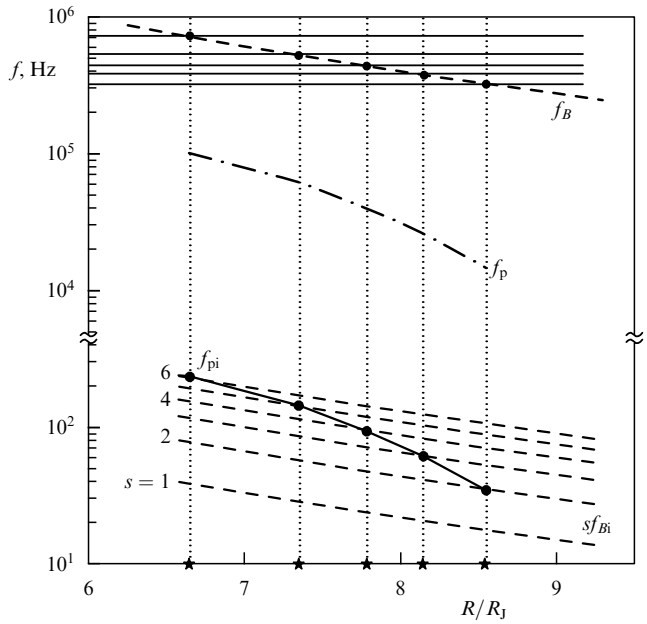

Figure 10. Model of the ZP source in kilometer radio emission from Jupiter whose dynamic spectrum is shown in Fig. 9 at the time marked by the dashed line [54]: the electron gyrofrequency f_B and the ion gyrofrequency harmonics sf_{Bi} with numbers $s = 2-6$ as a function of the distance $r = R/R_J$ from the center of Jupiter according to the VIP4 model [102]; the horizontal lines denote the observed ZP stripe frequencies at the marked time. Black dots show the DPR regions on the curves $sf_{Bi}(r)$. The stars on the abscissa mark the distances where the DPR regions with harmonics $s = 2-6$ are located.

The model proposed in [54] explains the characteristic features of the dynamic spectrum of the ZP in kilometer radio emission from Jupiter in a strong magnetic field ($\omega_p \ll \omega_B$): the presence of quasiharmonic stripes of enhanced intensity on the dynamic spectrum with the stripe spacing much smaller than the emission frequency and the increase in the stripe frequency spacing with frequency (due to the same signs of L_B and L_N in an inhomogeneous source).

We note that the Cassini mission recorded a ZP in radio emission from Saturn as well. The dynamic spectrum published in [51] represents a system of enhanced-intensity stripes parallel to the time axis, with the stripe spacing increasing with frequency. This phenomenon can possibly also be interpreted in terms of the DPR effect.

3.3 Zebra pattern in microwave emission from the Crab pulsar

The dynamic spectra of radio emission from the Crab pulsar obtained by Hankins and Eilek [55, 107] with the 300 m radio telescope Arecibo (Puerto Rico) using a dynamic spectrograph with a unique time resolution of fractions of a nanosecond contain valuable information on the source of radio emission and open new possibilities for reconstructing physical processes responsible for this emission. In particular, the fine structure of the dynamic spectrum in the form of relatively narrow quasiharmonic stripes drifting parallel in time significantly constrains the radio emission mechanisms. This situation is reminiscent of the theory of solar radio emission, when the appearance of the dynamic spectrograph in the 1950–1960s made it possible to classify and explain the origin of many solar radio bursts [66, 108, 109]. Moreover, the presence of a fine structure in the solar radio emission

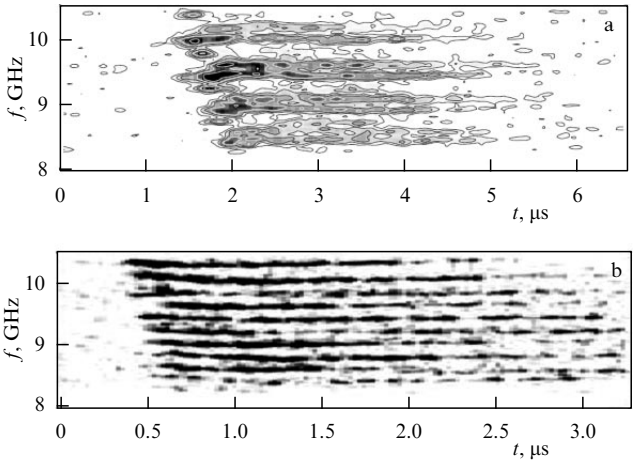

Figure 11. Examples of the dynamic spectra with the zebra pattern in the Crab pulsar microwave emission obtained with the 300-m Arecibo radio telescope with a unique time resolution of fractions of a nanosecond: [55] (a), [107] (b).

spectrum in the form of narrowband details enabled at that time discriminating between the synchrotron and plasma mechanisms of the broadband type-IV continuum in favor of the latter [2, 3, 84, 110]. It cannot be ruled out that the dynamic spectra of pulsars will shed light on the nature of their radio emission.

Dynamic spectra of short bursts in the interpulse of the polarized microwave radio emission from the Crab pulsar shown in Fig. 11 are in many respects very similar to the ZP in solar radio emission, shown in Fig. 5. Both structures represent a set of quasiharmonic enhanced emission stripes, with the stripe spacing much smaller than the emission frequency. In addition, the stripe spacing both in solar radio emission and in the emission from the Crab nebula is not constant: when moving from one stripe to another, it increases as the frequency increases [39, 55]. This property of the regular nonequidistance in both objects is very important in choosing the radio emission mechanism.

In solar radio emission, the ZP is observed in the wavelength range from several centimeters to several meters, and is most frequently registered in the decimeter range. The ZP from the Crab pulsar is detected in the microwave range. The ZP from the Sun with both a limited number of stripes (say, 5–7) [7, 14] and a very large number of stripes (more than ten) [13, 18] have been recorded. In the pulsar emission as well, both a few and many (more than ten) stripes have been recorded in one frequency interval (cf. Fig. 11a, b). In addition, in the case of the pulsar, the upper frequency limit can be related to the receiver band width: it is possible that the ZP spectrum extends to higher frequencies.

One mechanism of the origin of ZP spectra in radio emission from the Crab pulsar was proposed in [111], where the observed structure of the spectrum is related to the instability of relativistic electrons due to the anomalous Doppler effect, i.e., under the condition

$$\omega - k_{\parallel} v_{\parallel} = \frac{s\omega_B}{\gamma}\,, \qquad s < 0\,,$$

where $k_{\parallel}$ and $v_{\parallel}$ are the components of the wave vector and particle velocity along the magnetic field, s is the harmonic number, and γ is the Lorentz factor of emitting particles. For the emission from the source localized near the light cylinder, where the neutron-star magnetic field is $B \sim 10^6$ G, to be in the microwave range, it is necessary to assume the Lorentz factor of the emitting particles $\gamma \approx 7 \times 10^7$ and the plasma number density in the emitting region 3×10^5 times as high as the Goldreich–Julian density for a rotating neutron star magnetosphere [112]. In addition, ultrarelativistic electrons can hardly generate radio emission with narrowband details in the form of resolved ZP stripes with the stripe spacing much smaller than the emission frequency.

In [113], the appearance of the ZP in the Crab pulsar radio emission is explained by the modulation of the plasma wave amplification coefficient by a monochromatic magnetosonic wave. In other words, the problem of the ZP origin in radio emission is carried over from the problem of explaining the possibility of the existence of relatively weak magnetic fields in the source to the problem of generating monochromatic magnetosonic waves with a relatively large amplitude in the pulsar magnetosphere. We also note that in application to the solar ZP, this model is unable to explain the observed ordinary polarization of radio emission.

The similarity between the frequency ZP spectra in the solar radio emission and from the Crab pulsar suggests that the mechanisms responsible for the appearance of the 'striped' dynamic spectra can be similar in both cases. We believe [56] that the most likely reason for the appearance of dynamic ZP spectra is the DPR effect [1] (see also the paper by Hankins and Eilek [55], who mention this mechanism among others). However, the magnetic fields usually adopted for estimates (from $B \sim 10^{12}$ G near the neutron star surface to $B \sim 10^6$ G at the light cylinder) do not fall into the observed microwave range of the ZP spectrum: frequencies $f \approx (6-10)$ GHz, which correspond to relatively low electron cyclotron harmonics, are obtained for much smaller magnetic fields $B \sim 10^2$ G. We note that the possibility of DPR significantly constrains conditions in the source (see below for more details), which looks unusual for pulsar magnetosphere models discussed in the literature. However, narrowband ZP-like details in the dynamic spectrum and the ability of the DPR mechanism to explain the presence of parallel quasiharmonic stripes of enhanced emission with the stripe spacing increasing with frequency suggest the existence in the pulsar magnetosphere of a local source with a weak magnetic field and a relatively high plasma number density ($N \sim 10^{11}$ cm^{-3}).

Because the structure of the neutron star magnetosphere is actually unknown and there is no commonly accepted model, it is worth examining the mechanism of radio emission in the Crab pulsar with a ZP spectrum by putting aside the problem of formation of the required field structure and corpuscular plasma content for the DPR mechanism to operate. Following [56], we use only the observed properties of radio emission and rely only on the standard radio astronomical method of studying physical properties in the emission generation region based on the DPR effect to gain insight into the source parameters. This approach turned out to be very successful in application to the theory of solar radio emission generation: for example, fast-drifting type-III solar radio bursts were explained by the propagation of subrelativistic electron beams in the solar corona (without discussing the acceleration mechanism of these electrons), and powerful slowly drifting type-II bursts were associated with shocks (without inspecting the origin of these shocks).

3.3.1 Localization of the emission source with a zebra pattern. Figure 12 shows the mean profiles of the Crab pulsar emission at different frequencies as a function of the pulsar phase [114]. The schematic position of local emission sources in the pulsar projected on the equatorial plane are shown in Fig. 13 [56]. The main pulse is observed at the phase 70°. It is observed in X-ray, optical, and continuum radio emission. The interpulse is observed at the phase 215° in the same energy ranges. The ZP is detected only in the interpulse at the phase 205°, i.e., about 10° prior to the long-wave interpulse; no other components of the frequency spectrum are observed in the microwave precursor. These facts imply that the ZP is produced in a separate source whose parameters can significantly differ from those of the sources corresponding to the main pulse and interpulse and can vary in time as suggested, notably, by the different number of ZP stripes in one frequency interval in different events (Fig. 11a, b). This source, as well as all others, must be located inside the light cylinder, where the corotation regime governed by the magnetic field is realized (the coincidence of the rotation frequency of the emitting region and the spin frequency of the neutron star). Otherwise, the source phase would not be stable during long-term observations of the pulsar.

Following [115, 116], we assume that the averaged radio pulses are related to the relativistic formation of the pulsar emission beam from a rotating neutron star. Here, the emission source should be close to the light cylinder, where motion with a subluminal velocity provides a narrow emission beam. The relativistic model applied to all classes of radio pulses explains the appearance of emission bursts without artificial assumptions about the emission beam of individual sources. We note that in the relativistic model, the widths of the main pulse and the interpulse do not depend or depend weakly on the radio emission frequency (see [116]). This is well illustrated by observations of the Crab nebula pulsar. Here, of course, the specific radio burst profile reflects the specifics of radio emission generation related to the magnetic field configuration and plasma properties in each separate object. In the relativistic model of the ZP source, the source velocity V estimated from the rotational period and duration of the pulse (taking the duration shortening due to the orbital motion of the source into account [116]) is $\beta = V/c = 0.82$. With this velocity and the pulsar period $P = 3.3 \times 10^{-2}$ s, the source must be set at the distance $R = VP/2\pi \approx 1.3 \times 10^8$ cm from the neutron star spin axis, i.e., inside the light cylinder $R_L = c/\Omega = 1.6 \times 10^8$ cm, where $\Omega = 2\pi/P$ is the angular spin frequency of the star. It should be borne in mind, of course, that the sources can be located at different distances from the equatorial plane.

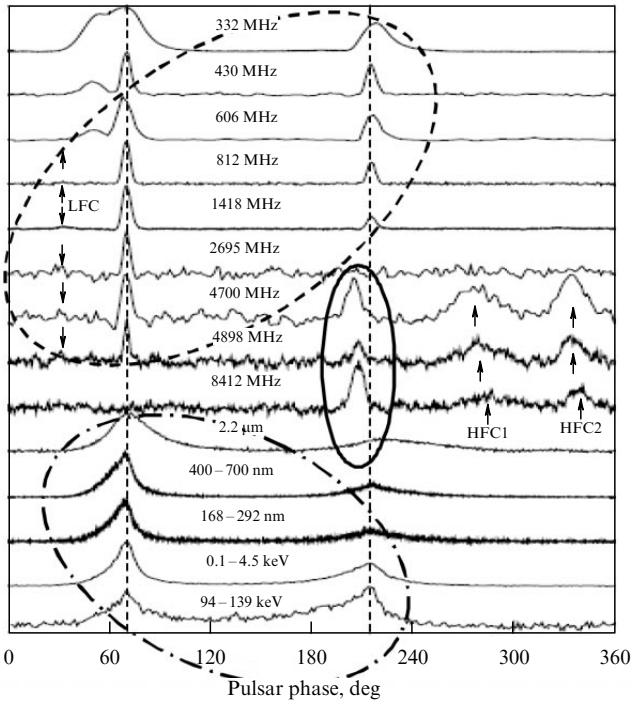

Figure 12. The averaged Crab pulsar emission profiles at different frequencies as a function of the pulsar phase [114]: the dashed oval is the source of optical and X-ray emission; the dashed-dotted oval is the source of continuum radio emission; the solid oval is the source of microwave emission with a zebra-like fine structure near the phase 205°.

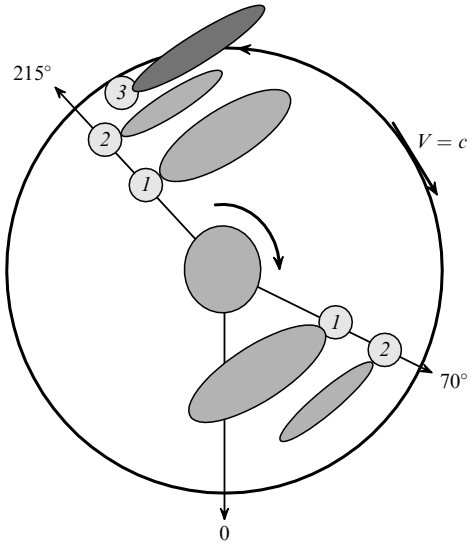

Figure 13. Position of local sources of optical, X-ray, and radio emission corresponding to the main pulse and interpulse of the Crab pulsar (projection on the equatorial plane). *1* — X-ray and optical emission source, *2* — continuum radio emission source, *3* — source of microwave emission with a ZP.

3.3.2 Plasma number density in a magnetic field in the source. By assuming that the ZP formation in the Crab pulsar is related to the DPR effect, we can estimate the required plasma number density and magnetic field strength in the source. The observed emission frequency f is related to the frequency f' in the source as [116]

$$f = f' \frac{\sqrt{1-\beta^2}}{1-\beta\cos\theta}, \tag{47}$$

where θ is the angle between the emission direction and the velocity in the observer frame. For $\beta = 0.82$ and $\cos\theta \approx 1$, this implies that the emission frequency in the source frame is

$$f' \approx 0.3 f. \tag{48}$$

For the observed frequency range $f = (6-10) \times 10^9$ Hz, we then have $f' \approx (1.8-3.0) \times 10^9$ Hz. If the ZP generation occurs near the plasma frequency $\omega_p = 2\pi f'$, the electron number density of the equilibrium nonrelativistic plasma in the source is $N \approx (0.9-1.2) \times 10^{11}$ cm^{-3}.

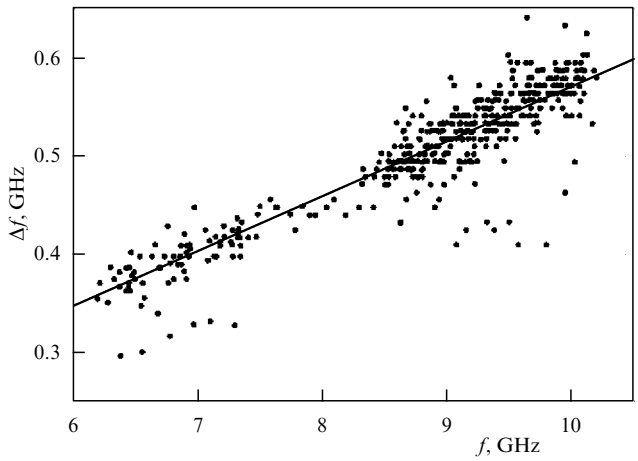

Figure 14. Frequency interval between neighboring stripes of the ZP as a function of frequency measured for 460 stripes of the ZP in 105 microwave emission pulses in 20 days of observations [55].

We now estimate the required magnetic field strength in the source. For the ZP in the distributed source model, the frequency interval between levels $s+1$ and s of the DPR is determined by formula (26). To relate the observed frequencies of the stripes to electron cyclotron harmonics and thus to estimate the magnetic field in the source with a ZP, we examine expression (26) in more detail. Setting $q = |L_B|/|L_N|$, we rewrite (26) in the form

$$F(q) \equiv \frac{\Delta f}{s f_B} = \frac{q}{\left|sq - (s+1)\right|} \,. \tag{49}$$

Clearly, the condition of visibility of resolved stripes $F(q) \ll 1$ constrains possible values of the parameter q. We take into account that the frequency spacing between stripes in the Crab radio emission is almost proportional to the emission frequency (Fig. 14):

$$\Delta f\ [\mathrm{GHz}] = 0.058(\pm 0.001)\, f\,[\mathrm{GHz}] - 0.007(\pm 0.011) \tag{50}$$

(the last term in this formula can be ignored). Hence, we find that

$$F(q) \approx 0.06 = \mathrm{const}\,. \tag{51}$$

A comparison of (49) and (51) shows that the ratio of the characteristic scales q must change across an inhomogeneous source: Eqns (49) and (51) uniquely relate the harmonic number and the parameter q: $17q = |sq - (s+1)|$. Because the ratio $q = |L_B|/|L_N|$ is unknown, we estimate the possible harmonic numbers in different cases.

For $q \ll 1$, Eqn (51) gives $q = (s+1)/17 \ll 1$, which holds only for harmonic numbers $s \ll 16$. This means that in the source in which the magnetic field changes with a coordinate faster than the electron number density, the ZP stripes represent low electron cyclotron frequency harmonics. In this case, the magnetic field is constrained within the limits 1.3×10^2 G $< B < 1.8 \times 10^3$ G (we recall that according to Fig. 3a, for $q < 1$ the lowest harmonic corresponds to the highest frequency). In reality, the magnetic field range that should include five observed harmonics in Fig. 11a is significantly narrower: if we assume, for example, that the harmonic number ranges from $s = 5$ to $s = 10$, the expected magnetic field interval is

$$2 \times 10^2\ \mathrm{G} < B < 7 \times 10^2\ \mathrm{G}\,. \tag{52}$$

In the case $q \gg 1$, the combination of conditions (50) and (51) yields only a lower bound on the harmonic number, $s > 17$, and hence

$$B < 2 \times 10^2\ \mathrm{G}\,. \tag{53}$$

As expected, both estimates give magnetic fields four orders of magnitude smaller than usually assumed in the pulsar vicinity (or the order of 10^6 G at the distance $R \approx 1.3 \times 10^8$ cm from a neutron star with the surface magnetic field $B \sim 10^{12}$ G; see [116]).

3.3.3 Plasma turbulence parameters. The plasma number density and magnetic field estimates in the ZP source given above are obtained by assuming that the observed radio emission frequency is close to the electron plasma frequency $\omega' \approx \omega_{\mathrm{p}}$, and the generation efficiency of emission at the double frequency $\omega' \approx 2\omega_{\mathrm{p}}$ is much smaller. This is because at high brightness temperatures of pulsar radio emission, the nonlinear decay of an electromagnetic wave at the double plasma frequency in two plasma waves with the frequency ω_L becomes significant. This process limits the growth of the emission brightness temperature at the double plasma frequency. Conversely, for emission near the plasma frequency $\omega' \approx \omega_{\mathrm{p}}$ at high brightness temperatures, the induced conversion of plasma waves into electromagnetic waves in scatterings on protons of the equilibrium plasma dominates, which leads to the exponential growth of the brightness temperature with the plasma wave energy density [79].

We now consider conditions under which the induced conversion of plasma waves into electromagnetic radiation in scattering on the equilibrium plasma ions can provide the observed brightness temperature of the ZP in microwave emission from the Crab pulsar. The linear size of the ZP source l can be deduced from the duration τ of the zebra stripes:

$$l \sim c\tau\sqrt{1-\beta^2} \sim 10^5\ \mathrm{cm}\,. \tag{54}$$

Then, in the source reference frame, the brightness temperature of radio emission is [116]

$$T_{\mathrm{b}} \approx \frac{\lambda^2 F}{\kappa}\left(\frac{R}{l}\right)^2 \frac{(1-\beta\cos\theta)^3}{(1-\beta^2)^2} \sim (10^{29}-10^{30})\ \mathrm{K} \tag{55}$$

at the wavelength $\lambda = 3$ cm ($f = 10$ GHz) for the observed flux $F \sim 100$ Jy at the distance $R \approx 2$ kpc.

The transformation of the excited plasma waves into electromagnetic waves due to Rayleigh scattering on equilibrium plasma particles occurs with energy conservation,

$$\omega_t - \omega = (\mathbf{k}_t - \mathbf{k})\mathbf{v}\,, \tag{56}$$

where ω_t and $\mathbf{k}_t$ are the frequency and wave vector of electromagnetic waves, and $\mathbf{v}$ is the velocity of scattering particles. The Rayleigh scattering is most effective on equilibrium plasma protons and results in the fundamental radio emission $\omega_t \approx \omega_{\mathrm{p}}$. Dispersion relations for plasma and electromagnetic waves for $\omega_{\mathrm{p}}/\omega_B \gg 1$ reduce

to the form

$$\omega^2 \approx \omega_{\rm p}^2 + 3v_T^2 k^2 , \qquad \omega_t^2 \approx \omega_{\rm p}^2 + k_t^2 c^2 . \tag{57}$$

Equations (56) and (57) determine the region of nonlinear interaction of an electromagnetic wave with the frequency ω_t and the excited plasma wave spectrum:

$$L = 3L_N \frac{v_T^2}{\omega_{\rm p}^2}(k_{\max}^2 - k_{\min}^2) \approx 3L_N \frac{v_T^2}{v_{\rm e}^2} , \tag{58}$$

where $k_{\max}$ and $k_{\min}$ determine the width of the excited plasma wave spectrum.

The transfer equation for the emission brightness temperature has the form [59]

$$\frac{{\rm d}T_{\rm b}}{{\rm d}l} = a - (\mu_N + \mu_{\rm c})T_{\rm b} , \tag{59}$$

where a is the emission coefficient, μ_N is the absorption (amplification) coefficient due to nonlinear processes, and $\mu_{\rm c}$ is the bremsstrahlung absorption coefficient. The solution of this equation is

$$T_{\rm b} = \frac{a}{\mu_{\rm c} + \mu_N}\left[1 - \exp\left(-\int_0^L (\mu_{\rm c} + \mu_N)\,{\rm d}l\right)\right] , \tag{60}$$

where L is given in (58). For Rayleigh scattering, the emission and absorption coefficients are [79]

$$a \approx \frac{\pi}{36}\frac{\omega_{\rm p}}{v_{\rm g}} m v^2 w , \qquad \mu_N \approx -\frac{\pi}{108}\frac{m}{m_{\rm i}}\frac{\omega_{\rm p}}{v_{\rm g}}\frac{v^2}{v_T^2} w , \qquad \mu_{\rm c} = \frac{\omega_{\rm p}^2}{\omega_t}\frac{\nu_{\rm ei}}{v_{\rm g}} \approx \frac{\nu_{\rm ei}}{v_{\rm g}} , \tag{61}$$

where $v_{\rm g}$ is the group velocity of electromagnetic waves and $w = W/N\kappa T$ is the ratio of the energy density of excited plasma waves to the thermal energy of equilibrium plasma. Because μ_N is negative, for $|\mu_N| > \mu_{\rm c}$, i.e., for a sufficiently high level of plasma turbulence, the exponential emission brightness temperature growth is possible (the maser effect). In this case,

$$T_{\rm b} \approx 3\frac{m_{\rm i}}{m} T \exp\left(\frac{\pi}{324}\frac{m}{m_{\rm i}}\frac{v^3}{v_T^3}\frac{\omega_{\rm p}}{v_T} Lw\right) . \tag{62}$$

As shown in Section 2, for ZP generation, the optimal ratio of the fast-particle velocity to the thermal velocity of plasma electrons is

$$\frac{v_{\rm e}}{v_T} \approx 10 - 20 . \tag{63}$$

In this case, assuming $\omega_{\rm p} \approx 2\pi \times 10^{10}$ GHz, $v_{\rm e}/v_T \approx 20$, $T \approx 10^6$ K, and $l \approx 10^5$ cm, we determine the brightness temperature of the observed ZP radio emission $T_{\rm b} \sim 10^{30}$ K, which can be explained by assuming that the ratio of the plasma wave energy density to the plasma thermal energy is, by the order of magnitude,

$$w = \frac{W_l}{N\kappa T} \approx 10^{-3} - 10^{-2} . \tag{64}$$

This value is below the strong turbulence generation threshold $w > w^* = 12v_T^2/v^2 \approx 3 \times 10^{-2}$ at which Langmuir solitons can appear, i.e., the condensation of plasma into clumps occurs, and plasma waves begin affecting the plasma dispersion properties. Therefore, the ZP in the pulsar microwave emission with fluxes below 100 Jy can apparently be considered in the weak plasma turbulence approximation.

3.3.4 Possible model of the zebra pattern source. We have argued above that the ZP in radio emission of the Crab pulsar is generated in a local source whose parameters can significantly differ from those of sources corresponding to the main pulse and the interpulse and that this source must be located inside the light cylinder where plasma is corotating with the neutron star magnetic field.

The next important point is related to the necessary existence in the corotating magnetosphere of plasma regions with a sufficiently weak magnetic field, which is needed to satisfy the condition $\omega_{\rm p} \gg \omega_B$ in the source. Possible magnetic field configurations were discussed in [56]. One of the examples is a magnetic trap with a flux tube filled by energetic electrons with nonequilibrium velocity components normal to the magnetic field, like the ZP source in the solar corona. At the top of such a trap, the field must be sufficiently weak ($\omega_{\rm p} \gg \omega_B$), which is required for the DPR instability. We note that the possibility of the existence of weak magnetic fields in the inner magnetosphere near the light cylinder was discussed in [112, 117, 118].

From the standpoint of the existence of local regions with a weak magnetic field in the Crab pulsar magnetosphere, a configuration in the form of a neutral current sheet seems to be more attractive [119]. Indeed, in the central part of the sheet, where the magnetic field is small and the plasma number density can be sufficiently high, it is easy to satisfy the weak anisotropy condition $\omega_{\rm p} \gg \omega_B$ for plasma, which is needed for the DPR effect. But in the neutral current sheet, the plasma number density and magnetic field gradients along the coordinate l are directed oppositely. Therefore, the ZP stripe spacing decreases as the frequency increases (Fig. 3d), in contradiction with observations. Therefore, a classical neutral current sheet seems to be unlikely to be the ZP source in the pulsar spectrum.

We now imagine that on top of a neutral current sheet, there is a transverse magnetic field $B_{\rm l}$, parallel to the gradient of the main layer parameters, which is weak compared with the field B_∞: $B_\infty \gg B_{\rm l}$. The corresponding magnetic field configuration shown in Fig. 15 resembles a strongly elongated magnetic trap. Next, we assume that this transverse magnetic field varies along the layer (along the coordinate m in Fig. 15), and energetic electrons occupy the central part of the layer. Clearly, if the electron number density N is also inhomogeneous along the coordinate m, DPR levels can arise due to the parameter inhomogeneity along the coordinate m. This variant of a neutral current sheet with a transverse magnetic

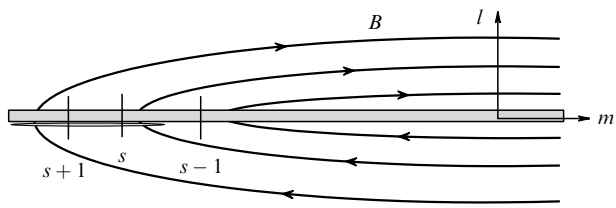

Figure 15. Location of the ZP source in a neutral current sheet with a weak transverse magnetic field; the gray region contains nonequilibrium electrons; the DPR surfaces are perpendicular to the main magnetic field in the sheet.

field or a strongly elongated magnetic trap is more favorable for the DPR effect in the pulsar magnetosphere. A relatively long-time generation of plasma waves in the magnetic trap (despite the short time of quasilinear relaxation) is ensured by the balance between the fast particle escape into the loss cone due to quasilinear effects and their replenishment due to the source of fast particles. As a result, plasma waves are generated in the trap with an effective increment smaller than its 'linear' value.

The dynamic spectra discussed here show two features: a harmonic structure and a regular nonequidistance of the harmonics. The first feature can be easily explained by the emission generation at harmonics of some fundamental frequency (for example, at the electron cyclotron harmonics in a homogeneous magnetic field), but the second peculiarity requires more: the generation of different harmonics in layers with different magnetic field strengths, i.e., in a source with an inhomogeneous magnetic field, which is provided by the enhanced emission generation at the DPR frequencies, in full agreement with the dynamic spectra of solar radio emission and the Crab pulsar emission. The magnetic field in the source must be sufficiently low: the relatively low harmonics of its electron gyrofrequency are comparable to the radio emission frequency. Such a magnetic field is ensured by its localization far from the equatorial plane of the rotating neutron star (but, of course, inside the light cylinder), or at lower heights in regions with a special configuration, like a neutral current sheet with a transverse magnetic field.

The observed dynamic spectrum of the Crab pulsar radio emission in the interpulse with discrete enhanced emission stripes can theoretically be caused by the instability of ion cyclotron waves. Invoking the ion cyclotron harmonics and lower hybrid resonance frequency to explain the emission from the pulsar magnetosphere is 'beneficial' in the sense that the magnetic fields that are required for these harmonics to be in the microwave range can be three orders of magnitude higher ($B \sim 10^5$ G) than in the case of electron cyclotron harmonics ($B \sim 10^2$ G). Such magnetic fields in the pulsar vicinity are more usual for neutron star magnetospheres. However, the possibility of detecting enhanced emission at the ion cyclotron harmonics should be investigated separately in connection with the problem of low-frequency radiation propagation outside the pulsar magnetosphere.

In this review, we considered ZP generation in the nonrelativistic electron–proton plasma. Presently, it is commonly accepted that pulsar magnetospheres are filled with electron–positron plasma. It is quite possible, however, that ions are also quite abundant in the pulsar magnetosphere. This possibility was mentioned already in the Goldreich and Julian paper [112]. Accelerating electric fields in the Crab pulsar were studied in detail in [119], where ion acceleration regimes were discovered with ion currents being possibly comparable with accelerated electron ones. The problem of the presence of the electron–ion (proton) plasma in pulsar magnetospheres needs further investigation; however, the presence of the ZP in the pulsar radio emission and its successful interpretation in terms of the model similar to that of the ZP in solar radio emission supports this possibility. As regards the ZP emergence in the electron–positron plasma, a preliminary analysis shows that the ZP can in principle arise in such a plasma as well, but the problem requires further investigation.

We also note that the weak anisotropy condition $\omega_p^2/\omega_B^2 \gg 1$ in plasma, which is needed for the DPR effect, can be written in the form

$$\frac{\omega_p^2}{\omega_B^2} \approx \frac{4\pi}{\omega_B P}\bar{\lambda} \gg 1\,, \tag{65}$$

where P is the pulsar spin period and $\bar{\lambda} = N/N_{GJ}$ is the ratio of the plasma number density in the source to the Goldreich–Julian density $N_{GJ} \approx B/ceT$, which characterizes the corotating charge density in the magnetosphere as $\rho_c \approx eN_{GJ}$ [112]. For magnetic fields in the ZP source $B \approx 50-100$ G, this condition takes the form

$$\bar{\lambda} = \frac{N}{N_{GJ}} \gg (2.5-5)\times 10^6\,. \tag{66}$$

The true values of the $\bar{\lambda}$ factor in pulsar magnetospheres are unknown. We can only state from the quasineutrality of the plasma that its value must be sufficiently large. The values $\bar{\lambda} > 10^5-10^6$ are assumed in the literature [111, 120–123] to match different pulsar emission mechanisms with observations. The ZP generation mechanism considered above may suggest that the $\bar{\lambda}$ factor in the pulsar magnetosphere can be even higher.

In connection with the use of neutron current sheets as a possible model of the observed ZP in microwave emission from the Crab pulsar, we note that there is no generally accepted model of the pulsar magnetosphere structure. Some papers use numerical simulations to show that a current sheet starts forming inside the light cylinder [124], while other papers argue that the current sheet cannot be formed inside the light cylinder [125]. We note that the present-day results of numerical simulations cannot yet serve as a robust argument favoring one model or another, because it is unknown, in particular, how certain the assumption about the dipole structure of the magnetic field is. In addition, current sheets in which the ZP is produced represent a sporadic structure in the pulsar magnetosphere, because the ZP itself is observed occasionally in the interpulse emission of the pulsar (Fig. 11a, b). Hopefully, further radio pulsar studies using dynamic spectrographs with a high frequency–time resolution will provide important information shedding light on the nature of radio pulsars and the properties of pulsar magnetospheres.

4. Experimental study of the kinetic instability of plasma in the electron–cyclotron discharge with DPR

Laboratory studies of the instability of nonequilibrium electron–cyclotron discharge (ECD) in open magnetic traps, which revealed a dramatic amplification of plasma wave generation and related radio emission to the DPR condition, were reported in [126–128].

In these experiments, a gyrotron with a frequency of 37.5 GHz, a power of 80 kW, and a pulse duration of 1 ms is the source of powerful microwave emission that produces and heats plasma in an ECD. For the stage of developed discharge, a cold plasma component (with the number density $N \sim 10^{13}$ cm^{-3} and the temperature $T \approx 300$ eV) with an isotropic velocity distribution and less dense hot electrons (the number density $N_e \sim 10^{10}-10^{11}$ cm^{-3} and the temperature $T_e \sim 100$ eV) with an anisotropic velocity distribution formed in the trap [126-128]. In this experiment, the cold background plasma determines the plasma wave

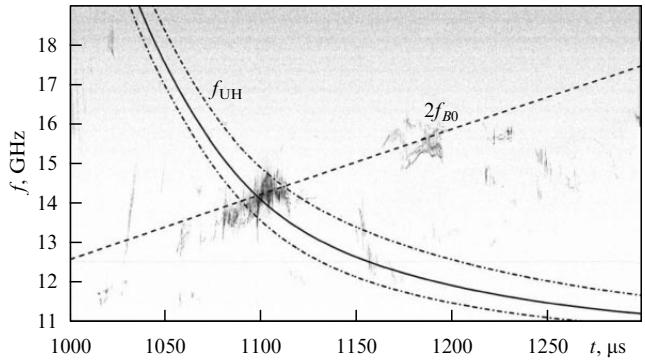

Figure 16. Dynamic spectrum of electromagnetic radiation accompanying the ECD plasma decay in a mirror trap; the dashed line shows the change in the $2f_{B0}$ frequency with time (f_{B0} is the electron cyclotron frequency on the longitudinal axis at the center of the magnetic trap); the solid line corresponds to the change in the upper hybrid resonance frequency f_{UH} during the plasma decay; the dashed-dotted line shows the dispersion in the determination of the frequency f_{UH} including the uncertainty (around 30%) in the background plasma temperature determination.

dispersion in the medium, and the hot electron component with a nonequilibrium velocity distribution provides instability and the generation of electromagnetic radiation.

Figure 16 shows the dynamic spectrum of the plasma emission immediately after quenching the gyrotron microwave emission. The analysis of experimental data enables determining the characteristic parameters of the instability. The sharp increase in emission occurs at a frequency of about $2f_{B0}$ (where f_{B0} is the electron cyclotron frequency at the magnetic trap center) and exhibits a pulse-periodic structure. The duration of radio bursts and synchronous current pulses of electrons precipitating from the trap is about 50 ns, and their period is about 200 ns. The high-frequency emission is observed at the instant during the decay when the upper hybrid resonance frequency f_{UH} becomes equal to the second electron cyclotron harmonic $2f_{B0}$ (see Fig. 16). This signals the DPR effect in the experiment.

We emphasize that the dynamic spectrum of radio emission in Fig. 16 does not have a diffusion character but consists of individual spikes, or 'pearls'. This feature of the dynamic spectrum is also frequently observed in the solar radio emission with a ZP [7, 18, 20, 28, 32, 34]. It also appears in the Crab pulsar radio emission and can be related to the quasiperiodic excitation of plasma waves due to the competition of the instability in the DPR region and the induced scattering of plasma waves on the background plasma particles [126]. Periodic injections of fast electrons from the trap, coinciding with the increased intensity of plasma waves, are related in this case to plasma wave generation by the normal Doppler effect, which results in fast electrons rapidly losing part of their 'transverse' energy. Ultimately, the plasma wave generation leads to electrons entering the loss cone and their subsequent precipitation from the magnetic trap.

5. Conclusion

The fine structure of radio emission spectra of astronomical objects provides rich information on physical processes in astrophysical plasmas. The ZP in dynamic radio emission spectra of the Sun, Jupiter, and the Crab pulsar discussed above suggests that DPR effectively operates in local sources in these objects.

A comparison of the observational properties of the ZP in solar radio emission with theoretical predictions gives clues to the magnetic field behavior in the corona (the correspondence to the force-free approximation when extrapolating photospheric fields into the upper atmosphere), the electron number density distribution in coronal loops (according to the barometric law), the fast magnetosonic oscillations of the magnetic tube, and the existence of trapped electrons with relatively high (but not relativistic) velocities. The interpretation of the ZP in the kilometer radio emission of Jupiter in terms of the DPR effect suggests the presence in the planet magnetosphere of a region outside the plasma layer containing the equilibrium electron–proton plasma with an admixture of trapped energetic electrons and protons.

Models of the ZP sources in the Sun and Jupiter fully correspond to the existing data on physical conditions in the solar corona and Jupiter's magnetosphere. The case is different for the explanation of the ZP in the Crab pulsar microwave emission. The quite unexpected detection of the ZP (after forty years of pulsar radio emission studies) opens new possibilities for solving the puzzle of pulsar radio emission. The complicated dynamic spectrum (a system of quasiregular stripes with a monotonic change in the distance between the neighboring harmonics) strongly constrains the radio emission mechanism and physical conditions in the emission generation region. Comparing dynamic spectra of solar radio emission and microwave emission from the Crab pulsar interpulse reveals a strong analogy. With the radio emission mechanism proposed 40 years ago [2–5] and based on the strong instability at DPR frequencies having been capable to explain the ZP structure in solar radio emission (in particular, owing to observations [22]), this opens the possibility of also applying it to magnetospheres of rotating neutron stars (the Crab pulsar, in particular). This mechanism can operate in nonequilibrium nonrelativistic electron–proton plasma immersed in a relatively weak magnetic field (compared to the strong magnetic fields of neutron stars). An important inference from this is that in addition to the relativistic plasma filling the neutron star magnetosphere, there can be regions with nonrelativistic plasma that can give rise to a zebra structure in the interpulse microwave emission.

Current relativistic pulsar models do not reflect the full complexity of conditions leading to the generation of radio emission with a complicated spectrum. These conditions ultimately justify the viability of proposed models of pulsar magnetospheres. As regards observations of radio pulsars, the study of the dynamic spectra of the Crab pulsars turns out to be as effective as the study of dynamic spectra of solar radio emission. Further investigations of pulsars with radiospectrographs should explain the abundance of frequency spectra with a fine structure similar to that observed in the Crab pulsar. Either this phenomenon is unique (which seems to be unlikely) or it is characteristic for other radio pulsars as well. In any case, undoubtedly, further studies of dynamic spectra initiated by Hankins and Eilek [55] open a new era in radio pulsar studies.

This study was supported by the RFBR grants 14-02-00766, 14-02-00133, and 16-02-00373, by the Program of Basic Research of the Presidium of RAS P-7, and partially by the RSF grant 16-12-10448 (Sections 3.3. and 4).

References

1. Pearlstein L D, Rosenbluth M N, Chang D B *Phys. Fluids* **9** 953 (1966)
2. Zheleznyakov V V, Zlotnik E Ya *Solar Phys.* **43** 431 (1975)
3. Zheleznyakov V V, Zlotnik E Ya *Solar Phys.* **44** 447 (1975)
4. Zheleznyakov V V, Zlotnik E Ya *Solar Phys.* **44** 461 (1975)
5. Kuijpers J *Astron. Astrophys.* **40** 405 (1975)
6. Elgarøy Ø *Astrophis. Norvegica* **7** 123 (1961)
7. Slottje C *Solar Phys.* **25** 210 (1961)
8. Chernov G P, Korolev O S, Markeev A K *Solar Phys.* **44** 435 (1975)
9. Bernold T *Astron. Astrophys. Suppl.* **42** 43 (1980)
10. Kuijpers J, in *Radio Physics of the Sun. Proc. of the Symp., College Park, Md., August 7–10, 1979* (IAU Symp. 86) (Dordrecht: D. Reidel Publ. Co., 1980) p. 341
11. Chernov G P, Zlobec P *Solar Phys.* **160** 79 (1995)
12. Chernov G P et al., in *Magnetic Fields and Solar Processes. The 9th European Meeting on Solar Physics, 12–18 September, 1999, Florence, Italy* (ESA SP-448, Ed. A Wilson) (Frascati: ESA, 1999) p. 765
13. Aurass H et al. *Astron. Astrophys.* **410** 1001 (2003)
14. Altyntsev A T et al. *Astron. Astrophys.* **431** 1037 (2005)
15. Kuznetsov A A *Astron. Astrophys.* **438** 341 (2005)
16. Chernov G P et al. *Astron. Astrophys.* **437** 1047 (2005)
17. Chen B, Yan Y *Solar Phys.* **246** 431 (2007)
18. Kuznetsov A A *Astron. Lett.* **33** 319 (2007); *Pis'ma Astron. Zh.* **33** 363 (2007)
19. Yan Y et al. *Publ. Astron. Soc. Jpn.* **59** S815 (2007)
20. Kuznetsov A A *Solar Phys.* **253** 103 (2008)
21. Melnik V N, Rucker H O, Konovalenko A A, in *Solar Physics Research Trends* (Ed. P Wang) (New York: Nova Sci. Publ., 2008) p. 287
22. Chen B et al. *Astrophys. J.* **736** 64 (2011)
23. Yu S, Yan Y, Tan B *Astrophys. J.* **761** 136 (2012)
24. Tan B et al. *Astrophys. J.* **744** 166 (2012)
25. Huang J, Tan B *Astrophys. J.* **745** 186 (2012)
26. Chernov G P et al. *Astron. Astrophys.* **538** A53 (2012)
27. Tan B et al. *Astrophys. J.* **780** 129 (2014)
28. Karlický M *Astron. Astrophys.* **561** A34 (2014)
29. Tan B et al. *Astrophys. J.* **790** 151 (2014)
30. Kaneda K et al. *Astrophys. J.* **808** L45 (2015)
31. Chernov G P *Space Sci. Rev.* **127** 195 (2006)
32. Chernov G P *Res. Astron. Astrophys.* **10** 821 (2010)
33. Chernov G P *Fine Structure of Solar Radio Bursts* (Berlin: Springer, 2011)
34. Chernov G P, arXiv:1512.06311
35. Zlotnik E Ya *Sov. Astron.* **21** 744 (1977); *Astron. Zh.* **54** 1309 (1977)
36. Berney M, Benz A O *Astron. Astrophys.* **65** 369 (1978)
37. Winglee R M, Dulk G A *Astrophys. J.* **307** 808 (1986)
38. Kuznetsov A A, Tsap Yu *Solar Phys.* **241** 127 (2007)
39. Zlotnik E Ya et al. *Astron. Astrophys.* **410** 1011 (2003)
40. Yasnov L V, Karlický M *Solar Phys.* **219** 289 (2004)
41. Zlotnik E Ya *Central Eur. Astrophys. Bull.* **33** 281 (2009)
42. Zlotnik E Ya, Sher E M *Radiophys. Quantum Electron.* **52** 88 (2009); *Izv. Vyssh. Uchebn. Zaved. Radiofiz.* **52** 95 (2009)
43. Zlotnik E Ya, Zaitsev V V, Aurass H *Astron. Lett.* **37** 508 (2011); *Pis'ma Astron. Zh.* **37** 555 (2011)
44. Zlotnik E Ya, Zaitsev V V, Aurass H *Central Eur. Astrophys. Bull.* **36** 161 (2011)
45. Zlotnik E Y *Solar Phys.* **284** 579 (2013)
46. Zlotnik E Y, Zaitsev V V, Altyntsev A T *Solar Phys.* **289** 233 (2014)
47. Yasnov L V, Karlický M *Solar Phys.* **290** 2001 (2015)
48. Zlotnik E Y et al. *Solar Phys.* **290** 2013 (2015)
49. Litvinenko G V et al. *Icarus* **272** 80 (2016)
50. Kurth W S et al., in *Planetary Radio Emissions V, Proc. of the 5th Intern. Workshop, Graz Austria, April 2–4, 2001* (Eds H O Rucker, M L Kaiser, Y Leblanc) (Vienna: Austrian Acad. of Sci. Press, 2001) p. 15
51. Menietti J D et al. *J. Geophys. Res. Space Phys.* **113** A05213 (2008)
52. Titova E E et al. *Geophys. Res. Lett.* **34** L02112 (2007)
53. Kuznetsov A A, Vlasov V G *Planet. Space Sci.* **75** 167 (2013)
54. Zlotnik E Ya, Shaposhnikov V E, Zaitsev V V *J. Geophys. Res.* **121** 5307 (2016)
55. Hankins T H, Eilek J A *Astrophys. J.* **670** 693 (2007)
56. Zheleznyakov V V, Zaitsev V V, Zlotnik E Ya *Astron. Lett.* **38** 589 (2012); *Pis'ma Astron. Zh.* **38** 660 (2012)
57. Mikhailovsky A B *Theory of Plasma Instabilities I* (New York: Consultant Bureau, 1974); Translated from Russian: *Teoriya Plazmennykh Neustoichivostei I* (Moscow: Atomizdat, 1970)
58. Bekefi G *Radiation Processes in Plasmas* (New York: Wiley, 1966); Translated into Russian: *Radiatsionnye Protsessy v Plazme* (Moscow: Mir, 1971)
59. Zheleznyakov V V *Elektromagnitnye Volny v Kosmicheskoi Plazme* (Electromagnetic Waves in Cosmic Plasmas) (Moscow: Nauka, 1977)
60. Zheleznyakov V V *Radiation in Astrophysical Plasmas* (Dordrecht: Kluwer Acad. Publ., 1996); Translated from Russian: *Izluchenie v Astrofizicheskoi Plazme* (Moscow: Yanus-K, 1997)
61. Akhiezer A I (Ed.) *Plasma Electrodynamics* (Oxford: Pergamon Press, 1975); Translated from Russian: *Elektrodinamika Plazmy* (Moscow: Nauka, 1974)
62. Stix T H *The Theory of Plasma Waves* (New York: McGraw-Hill, 1962); Translated into Russian: *Teoriya Plazmennykh Voln* (Moscow: Atomizdat, 1965)
63. Tataronis J A, Crawford F W *J. Plasma Phys.* **4** 231 (1970)
64. Dory R A, Guest G E, Harris E G *Phys. Rev. Lett.* **14** 131 (1965)
65. Zlotnik E Ya *Radiophys. Quantum Electron.* **18** 1 (1975); *Izv. Vyssh. Uchebn. Zaved. Radiofiz.* **18** 5 (1975)
66. Zheleznyakov V V *Radio Emission of the Sun and Planets* (Oxford: Pergamon Press, 1969); Translated from Russian: *Radioizluchenie Solntsa i Planet* (Moscow: Nauka, 1964)
67. Tsytovich V N *Non-Linear Effects in a Plasma* (New York: Plenum Press, 1970); Translated from Russian: *Nelineinye Effekty v Plazme* (Moscow: Nauka, 1967)
68. Tsytovich V N *Theory of Turbulent Plasma* (Berlin: Springer, 1977); Translated from Russian: *Teoriya Turbulentnoi Plazmy* (Moscow: Atomizdat, 1971)
69. Ginzburg V L, Zheleznyakov V V *Sov. Astron.* **2** 653 (1958); *Astron. Zh.* **35** 694 (1958)
70. Zheleznyakov V V, Zaitsev V V *Sov. Astron.* **14** 47 (1970); *Astron. Zh.* **47** 60 (1970)
71. Zheleznyakov V V, Zaitsev V V *Sov. Astron.* **14** 250 (1970); *Astron. Zh.* **47** 308 (1970)
72. Wild J P, Smerd S F, Weiss A A *Annu. Rev. Astron. Astrophys.* **1** 291 (1963)
73. Melrose D B, Sy W *Aust. J. Phys.* **25** 387 (1972)
74. Melrose D B, Dulk G A, Smerd S F *Astron. Astrophys.* **57** 279 (1978)
75. Melrose D B, Dulk G A, Gary D E *Proc. Astron. Soc. Aust.* **4** 50 (1980)
76. Zlotnik E Ya *Astron. Astrophys.* **101** 250 (1981)
77. Ginzburg V L, Zheleznyakov V V *Sov. Astron.* **3** 235 (1959); *Astron. Zh.* **36** 233 (1959)
78. Fomichev V V, Chertok I M *Sov. Astron.* **12** 21 (1968); *Astron. Zh.* **45** 28 (1968)
79. Zaitsev V V, Stepanov A V *Solar Phys.* **88** 297 (1983)
80. Shafranov V D, in *Reviews of Plasma Physics* Vol. 3 (Ed. M A Leontovich) (New York: Consultants Bureau, 1963) p. 1; Translated from Russian: in *Voprosy Teorii Plazmy* Iss. 3 (Ed. M A Leontovich) (Moscow: Gosatomizdat, 1963) p. 3
81. Manley J M, Rowe H E *Proc. IRE* **44** 904 (1956)
82. Pikel'ner S B, Gintsburg M A *Sov. Astron.* **7** 639 (1964); *Astron. Zh.* **40** 842 (1963)
83. Zaitsev V V *Sov. Astron.* **9** 572 (1966); *Astron. Zh.* **42** 740 (1965)
84. Zaitsev V V, Stepanov A V *Astron. Astrophys.* **45** 135 (1975)
85. Aurass H et al. *Solar Phys.* **190** 267 (1999)
86. Aurass H, Klein K-L *Astron. Astrophys. Suppl.* **123** 279 (1997)
87. Klein K-L et al. *Astron. Astrophys.* **320** 612 (1997)
88. Manoharan P K et al. *Astrophys. J.* **468** L63 (1997)
89. Newkirk G *Astrophys. J.* **131** 983 (1961)
90. Trakhtengerts V Yu *Geomagn. Aeronom.* **8** 263 (1968); *Geomagn. Aeronom.* **8** 966 (1968)
91. Zaitsev V V *Radiophys. Quantum Electron.* **13** 661 (1970); *Izv. Vyssh. Uchebn. Zaved. Radiofiz.* **13** 837 (1970)
92. Zlotnik E Y et al. *Solar Phys.* **255** 273 (2009)
93. Rosenberg H *Solar Phys.* **25** 188 (1972)
94. Chiuderi C, Giachetti R, Rosenberg H *Solar Phys.* **33** 225 (1973)

95. Zlotnik E Ya *Radiophys. Quantum Electron.* **19** 337 (1976); *Izv. Vyssh. Uchebn. Zaved. Radiofiz.* **19** 481 (1976)
96. Zlotnik E Y, in *Trudy Vserossiiskoi Konf. po Solnechno-zemnoi Fizike, Posvyashchennoi 50-letiyu ISZF SO RAN, 28 – 30 Iyunya 2010, Irkutsk* (Proc. All-Russ. Conf. on Solar-terrestrial Physics Devoted to 50-years Anniversary of Institute of Solar-Terrestrial Physics) Vol. 16 (Irkutsk: Institute of Solar-Terrestrial Physics, 2011) p. 49
97. LaBelle J et al. *Astrophys. J.* **593** 1195 (2003)
98. Ledenev V G, Yan Y, Fu Q *Solar Phys.* **233** 129 (2006)
99. Yurovsky Yu *Solar Phys.* **258** 267 (2012)
100. Barta M, Karlický M *Astron. Astrophys.* **450** 359 (2006)
101. Laptukhov A I, Chernov G P *Plasma Phys. Rep.* **32** 866 (2006); *Fiz. Plazmy* **32** 939 (2006)
102. Laptukhov A I, Chernov G P *Plasma Phys. Rep.* **35** 160 (2009); *Fiz. Plazmy* **35** 185 (2009)
103. Laptukhov A I, Chernov G P *Plasma Phys. Rep.* **38** 560 (2012); *Fiz. Plazmy* **38** 613 (2012)
104. Connerney J E et al. *J. Geophys. Res.* **103** 11929 (1998)
105. Bagenal F, Delamere P A *J. Geophys. Res.* **116** A05209 (2011)
106. Zarka P *J. Geophys. Res.* **103** 20159 (1998)
107. Hankins T H, Rankin J M, Eilek J A, Astro2010: Science White Papers No. 112 (2010)
108. Wild J P, McCready L L *Austral. J. Sci. Res. A* **3** 387 (1950)
109. Kundu M R *Solar Radio Astronomy* (New York: Interscience Publ., 1965)
110. Stepanov A V *Sov. Astron.* **17** 781 (1974); *Astron. Zh.* **50** 1243 (1973)
111. Lyutikov M *Mon. Not. R. Asron. Soc.* **381** 1190 (2007)
112. Goldreich P, Julian W H *Astrophys. J.* **157** 869 (1969)
113. Karlický M *Astron. Astrophys.* **552** A90 (2013)
114. Moffett D A, Hankins T H *Astrophys. J.* **468** 779 (1996)
115. Smith F G *Nature* **223** 934 (1969)
116. Zheleznyakov V V *Astrophys. Space Sci.* **13** 74 (1971)
117. Beskin V S *Phys. Usp.* **42** 1071 (1999); *Usp. Fiz. Nauk* **169** 1169 (1999)
118. Beskin V S, Gurevich A V, Istomin Ya N *Sov. Phys. JETP* **58** 235 (1983); *Zh. Eksp. Teor. Fiz.* **85** 401 (1983)
119. Harris E G *Nuovo Cimento* **23** 115 (1962)
120. Hirotani K *Astrophys. J.* **652** 1475 (2006)
121. Lyutikov M *Mon. Not. R. Asron. Soc.* **353** 1095 (2004)
122. Lyutikov M, Tompson C *Astrophys. J.* **634** 1223 (2005)
123. Muslimov A G, Harding A K *Astrophys. J.* **588** 403 (2003)
124. Gruzinov A, arXiv:1111.3377
125. Li J, Spitkovsky A, Tchekhnovsky A *Astrophys. J. Lett.* **746** L24 (2012)
126. Viktorov M E et al. *Radiophys. Quantum Electron.* **57** 849 (2015); *Izv. Vyssh. Uchebn. Zaved. Radiofiz.* **57** 947 (2014)
127. Vodopyanov A V et al. *JETP* **104** 296 (2007); *Zh. Eksp. Teor. Fiz.* **131** 330 (2007)
128. Vodop'yanov A V et al. *Tech. Phys. Lett.* **25** 588 (1999); *Pis'ma Zh. Tekh. Fiz.* **25** (14) 90 (1999)